공학석사 학위논문

# Estimation of Net Retention Time of Solute in Storage Zones for Mixing Analysis in Streams

# 자연하천에서 물질 혼합해석을 위한 저장대에서의 정체시간분포 산정

2022년 2월

서울대학교 대학원

건설환경공학부

김 병 욱

# Estimation of Net Retention Time of Solute in Storage Zones for Mixing Analysis in Streams

자연하천에서 물질 혼합해석을 위한 저장대에서의
정체시간분포 산정

지도교수 서 일 원

이 논문을 공학석사 학위논문으로 제출함

2021년 10월

서울대학교 대학원

건설환경공학부

김 병 욱

김병욱의 공학석사 학위논문을 인준함

2021년 12월

위 원 장 _____ (인)

부위원장 _____ (인)

위 원 _____ (인)

# ACKNOWLEGEMENTS

I would like to thank my adviser, Professor Il Won Seo, for his valuable guidance and continuous encouragement. I attribute the achievements with this study to his support. I also thank the members of the thesis committee: Professor Young-Oh Kim, Professor Il Won Seo, and Professor Yong Sung Park, who have taken the time to review and discuss the dissertation. Further, I would like to thank the colleagues from the Environmental Hydraulic Lab. in Seoul National University, and the members at Chemical Accident Response R&D program (2018001960001) for their contribution on the field work. It has been a unique opportunity to be part of the team conducting tracer experiments and to be able to use the data for this research. I would also like to express my appreciation to Professor Ian Guymer in the University of Sheffield for his kind advise on this work.

ABSTRACT OF DISSERTATION

# Estimation of Net Retention Time of Solute in Storage Zones for Mixing Analysis in Streams

by

Byunguk Kim

Master in Civil and Environmental Engineering
Seoul National University

Professor Il Won Seo, Advisor

The solute propagation along stream flow cannot be interpreted only by hydrodynamic properties of surface flow due to the influence from surrounding storage zones of the stream. To analyze this unidentified storage effect, various transient storage models have been proposed for recent decades. The time dependent behavior of solute within the storage zone was often modeled a conceptualized retention time function added to conventional advection-dispersion equation. The validity of these models has been predominantly demonstrated with tracer breakthrough curves measured in surface flow. However, the storage effect is less responsible for the breakthrough curve behavior than in-stream flow dynamics. For

model validation purpose, tracer behavior only within storage zones should be investigated. The present study is aimed at quantifying the time-dependent storage effect, herein termed the net retention time distribution (NRTD), from tracer measurements at the flow zone using a deconvolution technique with filtering in the Fourier domain. The results showed that the deconvolved NRTDs successively represented the temporal behavior of the tracer in the storage zones without significant distortion in the observed breakthrough curves. Using the estimates of NRTD, we evaluated the validity of first-order mass transfer and its parameters of the transient storage model (TSM), which is the most widely-used storage zone model. The simulation results of the parameter-optimized TSM underestimated the inherent storage effect by as much as an average 44 %. It is also noteworthy that the larger net retention time scale the channel has, the larger discrepancy the TSM's exponential retention time function could yield.

Keywords: solute transport, non-Fickian transport, transient storage model, net retention time function, tracer test, biodegradation

*Student Number* : 2020-22143

TABLE OF CONTENTS

LIST OF FIGURES

LIST OF TABLES

# LIST OF SYMBOLS

| Variable | Description | Units |
|---|---|---|
| Alphabetical symbols | | |
| $A$ | cross-sectional area of surface flow | $m^2$ |
| $A_s$ | cross-sectional area of storage zone | $m^2$ |
| $C$ | concentration | $mg\ m^{-3}$ |
| $\bar{C}$ | Laplace transformed concentration in surface flow zone | $mg\ m^{-3}$ |
| $C_{ini}$ | initial concentration | $mg\ m^{-3}$ |
| $C_s$ | concentration in storage zone | $mg\ m^{-3}$ |
| $\overline{C_s}$ | Laplace transformed concentration in storage zone | $mg\ m^{-3}$ |
| $E_z$ | transversal mixing coefficient | $m^2 s^{-1}$ |
| $F(\cdot)$ | filtering operator | |
| $g$ | memory function | $s^{-1}$ |
| $i$ | imaginary number | |
| $H$ | flow depth | $m$ |
| $L_0$ | required distance to complete transversal and vertical mixing | $m$ |
| $M$ | total introduced mass | $g$ |
| $N$ | number of particles | |
| $N_f$ | filtering order of the Butterworth filter | |
| $N_{obs}$ | number of observations | |
| $n$ | number of injection points | |
| $Q$ | flow discharge | $m^3 s^{-1}$ |
| $r$ | residence time distribution | $s^{-1}$ |
| $r_F$ | residence time distribution of Fickian behavior in time domain | $s^{-1}$ |
| $r_{nF}$ | residence time distribution of non-Fickian behavior in time domain | $s^{-1}$ |

| | | |
|---|---|---|
| $\widetilde{r_F}$ | residence time distribution of Fickian behavior in Fourier domain | $s^{-1}$ |
| $\widetilde{r_{nF}}$ | residence time distribution of non-Fickian behavior in Fourier domain | $s^{-1}$ |
| $r_{obs}$ | observed residence time distribution | $s^{-1}$ |
| $r_{sim}$ | simulated residence time distribution | $s^{-1}$ |
| $T_c$ | characteristic time ($\equiv x/u$) | $s$ |
| $T_h$ | retention time scale parameter | $s$ |
| $t$ | time | $s$ |
| $U_*$ | shear velocity | $m\,s^{-1}$ |
| $x$ | distance in streamwise direction | $m$ |
| $D_L$ | longitudinal dispersion coefficient | $m^2 s^{-1}$ |
| $u$ | current velocity | $m\,s^{-1}$ |
| $W$ | mean top-width of channel | $m$ |
| $s$ | Laplace variable | |

Greek symbols

| | | |
|---|---|---|
| $\alpha$ | mass exchange coefficient | $s^{-1}$ |
| $\varepsilon$ | relative volumetric size of the storage zone to the flow zone | |
| $\varepsilon_a$ | allowed error rate | |
| $\Gamma$ | sink-source term for transient storage modeling | |
| $\varphi$ | retention time function | $s^{-1}$ |
| $\Phi$ | net retention time function in time domain | $s^{-1}$ |
| $\widetilde{\Phi}$ | net retention time function in Fourier domain | $s^{-1}$ |
| $\tau$ | dummy time variable | $s$ |
| $\omega$ | frequency | $s^{-1}$ |
| $\omega_c$ | cutoff frequency | $s^{-1}$ |
| $\omega_N$ | Nyquist frequency | $s^{-1}$ |

# LIST OF ABBREVIATIONS

| Abbreviation | Description |
|---|---|
| ADE | Advection-Dispersion Equation |
| EPA | Environmental Protection Agency |
| FFT | Fast Fourier Transform |
| FRF | Filter Response Function |
| GC | Gam Creek |
| NRTD | Net Retention Time Distribution |
| PDF | Probability Density Function |
| RTD | Residence Time Distribution |
| RTK-GPS | Real-Time Kinematic Global Positioning System |
| RWT | Rhodamine WT |
| TSM | Transient Storage Model |

# CHAPTER I

# INTRODUCTION

## 1.1 Motivation

Worldwide industrialization has caused a dramatic rise in chemical usage in industrial complexes, which has in turn led to spill accidents of harmful contaminant. In November 2014, a truck overturned and spilled 2,000 L of sulfuric acid into Nakdong River, the longest river in South Korea, and it resulted in severe damage to the aquatic ecosystem and water quality. Another 9 of the spill accidents occurred during last 30 years in Nakdong River. Such unpredictable accidents in rivers are especially serious since most water supply in South Korea is dependent on surface waters, such as rivers and reservoirs. Having recognized the problem, many engineers and researchers have required to understand contaminant behavior along with the stream flow, which is high-dimensional, multiscale, and nonlinear system. Hence, there have been a need for interpretable and generalizable solute transport models.

Such contaminant spilt into a stream is diluted along with its propagation downstream by molecular or turbulent diffusion or shear effect. However, the time and distance scale that it takes for complete dilution is extremely large. In 1991, the 70,000 L of metam sodium spilt in Sacramento River, California, was detected up to 55 km downstream for 26 days. In 2005, the 41,000 L of sodium hydroxide spillage spilt into Cheakamus River, Vancouver, killed 500,000 fishes in an 18 km section. In 2008, the

phenol split into Nakdong River, South Korea, was detected up to 78 km downstream. Due to the computational cost and input data requirement, and reliability in calibration, more than one dimensional models cannot be employed for such lone-distance propagation. Therefore, models for one-dimensional analysis have been used and developed despite significant uncertainties from their idealizations and assumptions.

Early understanding of solute mixing in flowing water is that it is dominated by two mechanisms: When a source of solute introduced into a stream, the peak point of solute cloud is transported by mean flow velocity and its cloud shape isotopically spreads. However, actual solute propagation is not that simple. Due to morphological influences such as pools, eddies, rocks, vegetations, bed materials or banks, low-velocity or stagnate regions are formed in streams and they transiently trap the solute and released after some retention time. Such in-stream structure is referred to as "storage zone" regardless of its shape, size, retention scale. The storage effect skews the contaminant cloud with long tails. In two- or three-dimensional simulation, such skewness can be reproduced by boundary shear effect of bottom or banks. While, in one-dimensional model, such skewness cannot be generated only by advection and diffusion. Hence, various one-dimensional models that can reproduce the storage effect have been developed for recent decades. However, it still remains challenging due to complexity and heterogeneity of in-stream storage zones. Therefore, intensive researches continues for deeper understanding of the storage effect.

In addition, since the rate of trapping from flow zone into storage zone is

much faster than that of releasing back to flow zone, various dissolved and suspended materials are concentrated in the storage zones. Likewise, the storage zones are habitable for microbes, so these zones are in turn a “hot spots” for biogeochemical activity. Therefore, knowing the storage mechanism is important to analysis of hosting chemical reaction, carbon stores, interaction with biofilms, algae blooming, and vegetation.

## 1.2 Problem Statement

The storage mechanism is typically considered and embedded into the conventional advection-diffusion model, and the anomalous storage effect is characterized with several parameters. The parameter-calibrated model yields the time-concentration curve, hereafter called the breakthrough curve (BTC), in the flow zone. Such storage-incorporated models have been validated by comparing the simulation result with the calibrated data to see how accurately it was fitted (see Table 1). However, there is a considerable problem with this method. Compared to the effects of advection and diffusion, the storage effect is less sensitive to forming breakthrough curves. In this respect, the inaccuracy of storage zone modeling may not be revealed in the breakthrough curves. Therefore, present study is arguing that the validity of the storage unit modeling should be demonstrated from the measurements that can represent the storage effect itself. However, it is difficult to identify the storage effect in streams due to the variability in forms and characteristics. This study aims to acquire

such data that can only represent the storage effect by excluding the effects of advection and diffusion from the tracer behavior observed in flow zone (see Fig. 1).

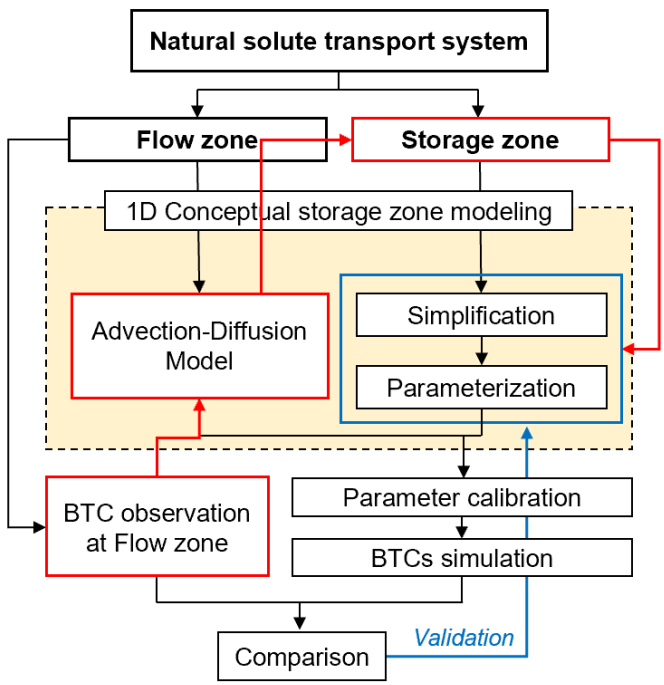


Figure 1. Typical way of storage mechanism modeling and validation

Table 1. Validation methods of existing storage zone modeling

| Model | Study | Validation with | Observed at | Accuracy |
|---|---|---|---|---|
| TSM | Bencala and Walters, 1983 | whole BTC | Surface flow | - |
| | Runkel and Broshears, 1991 | whole BTC | Surface flow | - |
| | Runkel, 1998 | whole BTC | Surface flow | - |
| | Gooseff et al, 2005 | whole BTC | Surface flow | - |
| APM | Elliott and Brooks, 1997 | whole BTC | Surface flow | relative error |
| Log-normal RTD | Worman et al., 2002 | BTC tail | Surface flow | relative error |
| Power-law RTD | Haggerty et al., 2002 | BTC tail | Surface flow | absolute error |
| TAD model | Meerschaert et al., 2008 | BTC tail | Surface flow | - |
| F-ADE | Deng et al., 2004, 2006 | whole BTC | Surface flow | - |
| CTRW | Boano et al., 2007 | BTC tail | Surface flow | - |
| STIR | Marion and Zaramella, 2005 | BTC tail | Surface flow | MSE |
| | Marion et al., 2008 | BTC tail | Surface flow | RMSE |
| | Bottacin-Busolin et al., 2011 | BTC tail | Surface flow | RMSE |
| | Zaramella et al., 2016 | whole BTC | Surface flow | RMSE |
| TSZM | Kerr et al., 2013 | whole BTC | Surface flow | - |
| Complex sorption kinetics | Liao et al., 2013 | BTC tail | Surface flow | RMSE |
| EAM model | Bottacin-Busolin, 2019 | BTC tail | Surface flow | RMSE |

* BTC is breakthrough curve of tracer concentration.

There have been previous studies that attempt to experimentally observed the tracer behavior in storage zones. Mignot et al. (2017) and Weitbrecht et al. (2008) investigated the tracer behavior within the artificial storage zone in laboratory scale. Gooseff et al. (2011), Jackson et al. (2012), and Sandoval et al. (2019) investigated the storage effect of the surface storage zones such as recirculation zones in side pockets in natural streams. However, these studies configured the storage zones to a specific shape and size, so their research results are somewhat localized, and it is difficult to expand and apply to those of natural streams due to the variability and heterogeneity of storage zones. Also, as shown in Fig. 2 and 3, the spatial-temporal scale of storage effect were much larger. Therefore, this study investigated the field-scale storage effect incorporating various types of storage zones.

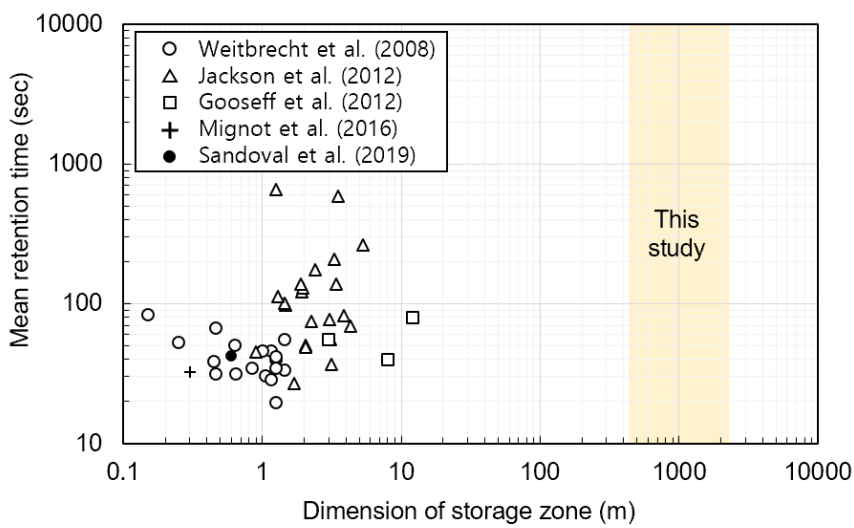


Figure 2. Parameter scales of existing studies and this study

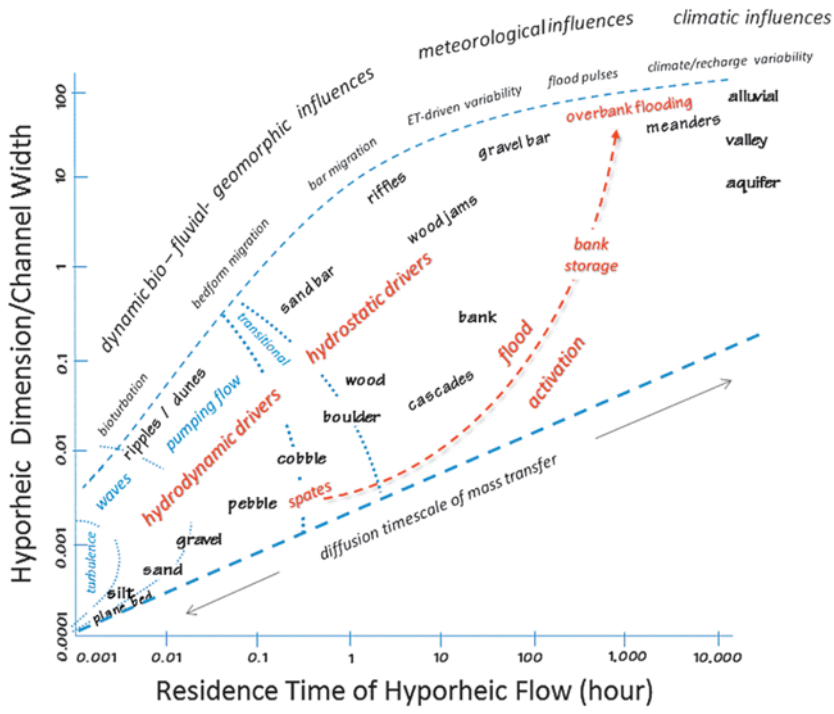


Figure 3 Spatial and temporal scaling of hyporheic flow (Boano et al., 2014)

# CHAPTER II

# THEORETICAL BACKGROUNDS

## 2.1 One-dimensional solute transport modeling

Models of any kind are of necessity idealized representations. Such idealization tend to concentrate on the dominant processes and the important features of the environment. As mentioned, passive scalar transport in flowing water body is commonly explained by two mechanisms: It is transport by main current, termed advection, and it spreads out by Brownian random motion of water, termed diffusion. This can be mathematically written as

$$\mathbf{q} = \mathbf{q}_a + \mathbf{q}_d \tag{1}$$

where $\mathbf{q}$, $\mathbf{q}_a$, $\mathbf{q}_d$ are the vector of the total mass flux, the advective mass flux, and the diffusive mass flux, respectively. A classical way to model the diffusion mechanism is to follow the Fick's law: It says that the diffusive flux of solute mass in a direction is proportional to the gradient of solute concentration along that direction. Fick's law can be written in vector notation as

$$\mathbf{q}_d = -D\nabla C \tag{2}$$

where $D$ is the proportionality coefficient in dimension of (length)$^2$/time, called the diffusion coefficient, and $C$ is the solute concentration defined as $C = \lim_{\Delta \to 0} \Delta M / \Delta V$, in which $\Delta M$ is the solute mass in elemental volume $\Delta V$. The advective mass flux is dependent on the current velocity, $\mathbf{q_a} = \mathbf{u}C$ in which $\mathbf{u}$ is the mean flow velocity vector with components $(u, v, w)$, so that the equation (1) becomes

$$\mathbf{q} = \mathbf{u}C + (-D\nabla C) \tag{3}$$

To satisfy conservation of mass, the mass flux of inflow and outflow in a volume must be equal the rate of mass change in the volume, $\partial C / \partial t = -\nabla \cdot \mathbf{q}$. Then, the equation (3) becomes

$$\frac{\partial C}{\partial t} + \nabla \cdot (C\mathbf{u}) = D\nabla^2 C \tag{4}$$

or, making use of the incompressible fluid assumption

$$\frac{\partial C}{\partial t} + \mathbf{u} \cdot \nabla(C) = D\nabla^2 C \tag{5}$$

The equation (5) are known as the advection-diffusion equation. Eq. (5) can be expanded in Cartesian coordinates as

$$\frac{\partial C}{\partial t} + u\frac{\partial C}{\partial x} + v\frac{\partial C}{\partial y} + w\frac{\partial C}{\partial z} = D\left(\frac{\partial^2 C}{\partial x^2} + \frac{\partial^2 C}{\partial y^2} + \frac{\partial^2 C}{\partial z^2}\right) \quad (6)$$

As mentioned, the $D$ was referred to as the diffusion coefficient and it represents the rate of isotropic separation of cloud. Among the various causes, the shear effect from advective velocity gradient will greatly exceed that caused by molecular or turbulent motion (Day, 1975; Fischer et al., 1979; Taylor, 1954). Hence, the separation rate can be represented by the shear flow dispersion and the $D$ will be hereafter termed the dispersion coefficient. It must be note that the shear dispersion in streams cannot be isotropic anymore because the velocity profiles in $x$-, $y$-, and z-direction are considerably different. Due to the boundary effects, the velocity variations in vertical and transverse direction are more dramatic than that in longitudinal direction. As shown in Figure 4, given enough time, the cross-sectional mixing will be complete sooner than the longitudinal mixing. Therefore, in the far field mixing analysis, $\partial C/\partial y$ and $\partial C/\partial z$ in Eq. (6) can be deemed to be zero, and the one-dimensional advection-dispersion equation (1D ADE) is derived with a cross-sectional averaged longitudinal velocity $U$ as below.

$$\frac{\partial C}{\partial t} + U\frac{\partial C}{\partial x} = D\frac{\partial^2 C}{\partial x^2} \quad (7)$$

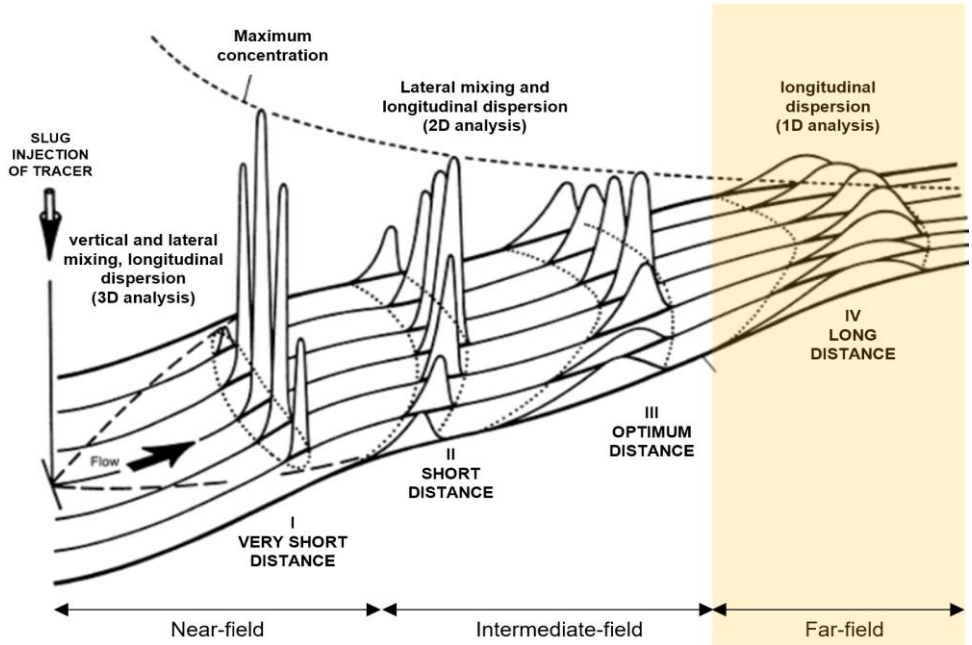


Figure 4. Mixing patterns and changes in concentration distribution (Kilpatrick & Wilson, 1989)

The premises for the dimensionality reduction are sometimes unacceptable because, in a reach-scale channel, such cross-sectional complete mixing may not happen, and many secondary details are omitted in the process. This margin of error could seem considerable. Even so, for the sake of the efficiency in numerical computation, applicability with the lack of available information, adaptability for relevant engineers, order-of-magnitude analysis, such approximation is worth much more than no answers.

Among the secondary factors in a streamflow, most considerable one is the morphological complexity. Solute transport is dominated not only by flow dynamics,

but also by interactions with surrounding storage zones of the stream. The role of storage zones in solute mixing is to impede its transport by trapping some solute particles, and after some retention time, releasing them back into the flow zone. Consequently, solute cloud is skewed with long tails as shown in Figure 5. Such skewness cannot be captured by Gaussian approximation of 1D ADE. Therefore, for recent decades, there have been many researches chasing the appropriate modelling incorporating the anomalous storage mechanism.

Figure 5. Tracer cloud behavior along Gam Creek, 2019.

## 2.2 Conceptualization of storage mechanism

Natural streams contain various types of storage zones in their form, size, and retention scale (see Figure 6), and such diversity makes the storage effect irregular and heterogeneous, resulting in difficult characterization in modeling. In three-dimensional analysis, such storage effect can be considered with the boundary effect of given bathymetric data and its dynamical interaction with flow, but it cannot in one-dimensional analysis. Rather the heterogeneous storage effect is predominantly idealized and parameterized with several parameters (see Table 2). Classical method is to add the additional sink-source term $\Gamma(t)$ into the 1D ADE as

$$\frac{\partial C}{\partial t} = -U\frac{\partial C}{\partial x} + D\frac{\partial^2 C}{\partial x^2} + \Gamma(t) \tag{8}$$

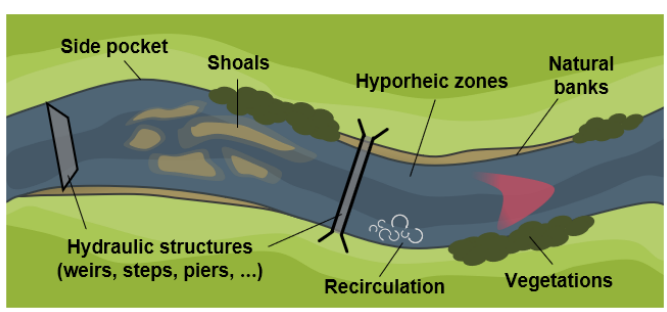


Figure 6. Typical storage zones in a natural stream

Table 2. General governing equations for transport of solutes in streams incorporating storage system

| Model | Papers | Description of Storage Process | Calibration Parameters | Governing Equation |
|---|---|---|---|---|
| Advection-Dispersion Equation (ADE) | Taylor, 1954; Elder, 1959 | None | 2 $[U,\ D]$ | $\frac{\partial C}{\partial t} = -U\frac{\partial C}{\partial x} + D\frac{\partial^2 C}{\partial x^2}$ |
| Fractional Advection Dispersion Equation (FADE) | Metzler and Klafter, 2000 | Heavy-tailed power law residence time distribution | 3 (S-FADE $[U,\ D_\alpha,\ \alpha]$, T-FADE $[U,\ D, \gamma]$) 4 (ST-FADE $[U,\ D_\alpha,\ \alpha,\ \gamma]$) | $\frac{\partial^\gamma C}{\partial^\gamma t} = -U\frac{\partial C}{\partial x} + D\frac{\partial^\alpha C}{\partial x^\alpha}$ |
| Transient Storage Model (TSM) | Bencala and Walter, 1983 | Finite volume, well-mixed storage zones | $4[U,\ D,\ \alpha,\ A/A_S]$ | $\frac{\partial C}{\partial t} = -U\frac{\partial C}{\partial x} + D\frac{\partial^2 C}{\partial x^2} + \alpha(C - C_s)$ |
| Multi-Rate Mass Transfer (MRMT) | Haggerty et al., 2000 | Any memory function or residence time distribution | Varies depending on memory function | $\frac{\partial C}{\partial t} = -U\frac{\partial C}{\partial x} + D\frac{\partial^2 C}{\partial x^2} + \int_0^t \frac{\partial C}{\partial \tau} g(\tau) d\tau$ |
| Continuous Time Random Walk (CTRW) | Boano et al., 2007 | Any memory function or residence time distribution | Varies depending on Residence time distribution | $\frac{\partial C}{\partial t} = \int_0^t \left(-U\frac{\partial C}{\partial x} + D\frac{\partial^2 C}{\partial x^2}\right) M(\tau) d\tau$ |
| Solute Transport In River (STIR) | Marion and Zaramella, 2005; 2008 | Any memory function or residence time distribution | Varies depending on how zones are specified | $C(t) = \int_0^t C_{\mathrm{AD}}(t)\, r_s(\tau) d\tau$ |

Due to simplicity and many existing relevant studies, Transient Storage Model (TSM) is most extensively used model since it can accurately simulate the skewness of breakthrough curve (BTC) (Bencala and Walters, 1983; Knapp and Kelleher, 2020). In words of Knapp and Kelleher (2020), *hydrologists, biogeochemists, and ecologists continue to leverage increasingly sophisticated field techniques to explore the storage and release of water, nutrients, and other solutes. But one thing has not changed: the ubiquitous use of one of the simplest and most straightforward conceptualizations of in- and near-stream transport, the transient storage model*. The TSM adopted the simple conceptualization that the retention mechanism can be described as equivalent to a first-order mass transfer. The model states that such mass transfer between surface flow zone and storage zone is induced by the concentration discrepancy between two domain and thus its governing equations were given by

$$\frac{\partial C}{\partial t} = \frac{\partial}{\partial x}\left(-UC + D\frac{\partial C}{\partial x}\right) + \alpha(C - C_s) \tag{9a}$$

$$C_s = \frac{\alpha}{\epsilon}(C_s - C) \tag{9b}$$

where $C_s(g\ m^{-3})$ is solute concentration within storage zone, $\epsilon$ is the relative volumetric size of the storage zone to the flow zone, and $\alpha(\mathrm{s}^{-1})$ is the mass exchange rate. Eq. (3) is a partial differential equation (PDE) due to the special-

temporal derivatives of the concentration. For the implicit equations, OTIS was proposed as a numerical solution (Runkel and Broshears, 1991; Runkel and Chapra, 1993; Runkel, 1998, Gooseff et al, 2005). The numerical analysis employed Finite Difference Method (FDM) which is a common method of resolving PDEs is to approximate the spatial derivatives, $\partial/\partial x$. The temporal derivative term was evaluated using Crank-Nikolson method with a centered difference approximation between both the current time and the future time. One of the advantages of the Crank-Nikolson method is that the one-dimensional model results in the formation of a tridiagonal coefficient matrix that can be efficiently solved using the Thomas Algorithm (Runkel and Broshears, 1991; Runkel and Chapra, 1993; Runkel, 1998).

Another method for the PDE solution is to derive the analytical solution in Laplace domain as the works of Kazezyılmaz-Alhan (2007) or Kim et al. (2021). Within the governing equations, once the time variable is converted to the Laplace variable, $s$, the Laplace transformed concentration in the storage zone (notated as $\overline{C_S}$) have a linear relationship with respect to the transformed flow zone concentration, $\bar{C}$ as Eq. (5).

$$K\frac{\partial^2 \bar{C}}{\partial x^2} - U\frac{\partial \bar{C}}{\partial x} + \alpha\overline{C_S} - \alpha\bar{C} - C(t=0) = 0 \tag{10}$$

$$\overline{C_S} = \frac{\frac{\alpha}{\epsilon}}{\frac{\alpha}{\epsilon} + s}\bar{C} \tag{11}$$

in which

$$\bar{C}(x,s) = \mathcal{L}[C(x,t)] = \int_0^\infty e^{-st} C dt \tag{12}$$

Substituting Eq. (5) into Eq. (4), the governing equation for the flow zone becomes a form of homogeneous ordinary differential equation (ODE), as:

$$D_L \frac{d^2\bar{C}}{dx^2} - u\frac{d\bar{C}}{dx} + \left(\frac{\alpha/\epsilon}{\alpha/\epsilon + s}\bar{C} - \alpha + -s\right)\bar{C} = 0 \tag{13}$$

Following the work of Kazezyılmaz-Alhan (2007), the general solution of the ODE was obtained, as:

$$\bar{C}(x,s) = \bar{C}(0,s)\exp\left[\left(\frac{u - \sqrt{u^2 - 4D_L\left(\frac{\alpha/\epsilon}{\alpha/\epsilon + s} - \alpha - s\right)}}{2D_L}\right)x\right] \tag{14}$$

The boundary condition was set as the Laplace transformed Heaviside function, signifying that the contaminant is introduced from time $t_1$ to $t_2$ with concentration of $C_{ini}$.

$$\bar{C}(0,s) = \frac{C_{ini}}{s}[\exp(-t_1 s) - \exp(-t_2 s)] \quad (15)$$

For inversion of the Laplace transform, the approximation polynomials, which are precalculated, are normally listed in tables. However, because we are unable to easily increase the order of the polynomials, the numerical inversion method based on the Bromwich integral was employed in this study to analyze the Laplace transform of the solution (Valsa and Brančik, 1998).

Kim et al. (2021a) showed the comparison of simulated BTC from the numerical model and the analytical solution with synthetic data. As input conditions, $Q$, $D_L$, $A$, $A_s$, and $\alpha$ were assumed to be 10 cms, 10 $m^2$ $s^{-1}$, 20 $m^2$, 5 $m^2$, and $10^{-5}$ $sec^{-1}$, respectively. 1 ppm of conservative solute were released at the inlet for 30 seconds, and simulated BTCs were compared at sections 500 m, 1,000 m, and 1,500 m downstream of the inlet (notated as S1, S2, and S3, respectively). The results revealed that both solutions yielded nearly identical results with a determination coefficient (R2) of over 0.99 at all sections, as plotted in Figure 7.

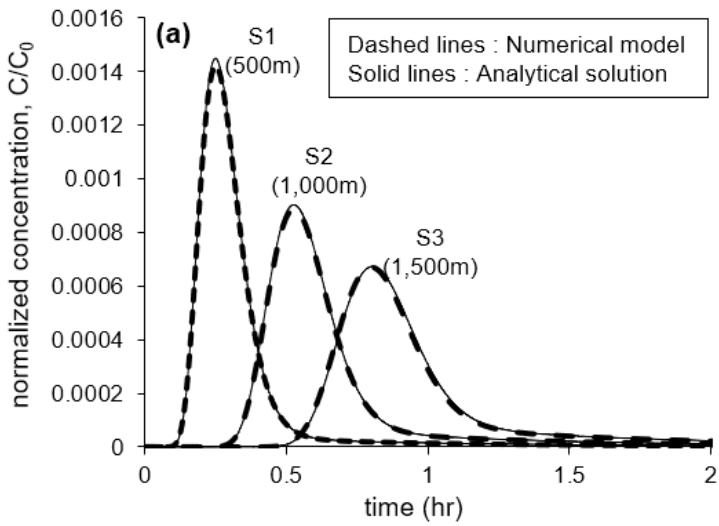


Figure 7. Comparison of simulation results of the numerical model and the analytical (Kim et al., 2021a).

As an relevant approach, time-dependent storage effect is often mathematically represented by the concept of residence time distribution (Haggerty et al., 2000), hereafter referred to as "retention time distribution", to differentiate it from that of the flow zone. The retention time indicates the time it takes for solute particles trapped in a storage zone to be released. Including Haggerty et al. (2000), several studies presented a model structure to characterize the storage mechanism in which the retention time distribution was defined as a memory function, and summarized the various memory function formulae (Boano et al., 2007; Drummond et al., 2012; Haggerty et al., 2002; Meerschaert et al., 2008). Afterwards, analogous conceptualizations were proposed, such as STIR (Bottacin-Busolin et al., 2011, 2021; Marion et al., 2008; Marion & Zaramella, 2005), or CTRW (Boano et al., 2007). The

transient storage model (TSM) is a retention time-based model in which an exponential memory function is embedded (Gooseff et al., 2011; Haggerty et al., 2000; Marion et al., 2008). Due to its structural simplicity and low computational cost, the TSM has many existing relevant studies and is the most established one-dimensional solute transport model. However, recent studies have argued that such exponential retention time distribution assumed by TSM framework is suitable for storage zones where the mass exchange rate is relatively fast, such as surface dead zone or thin surface layer of the hyporheic zone (Hart, 1995; Marion et al., 2008; Marion & Zaramella, 2005), and in turn poorly approximates the tailing behavior of tracer cloud in natural streams (Marion et al., 2008; Gooseff et al., 2003; Haggerty et al., 2002; Kim et al., 2021; Knapp & Kelleher, 2020) (see Figure 8. Simulation results from previous studies (a) Haggerty et al. (2002) (b) Gooseff et al. (2003) (c) Marion et al. (2008)). It is because, in storage zones of natural streams, the retention time scale could be much larger. It could range from seconds to tens of years in a hyporheic zone depending on bed materials and hyporheic dimension (Boano et al., 2014). Hence, the TSM formulation may underestimate the inherent storage effect of natural streams. This discrepancy also leads to difficulty in determining its parameters, which still relies on optimization techniques (Kim et al., 2021; Marion et al., 2002).

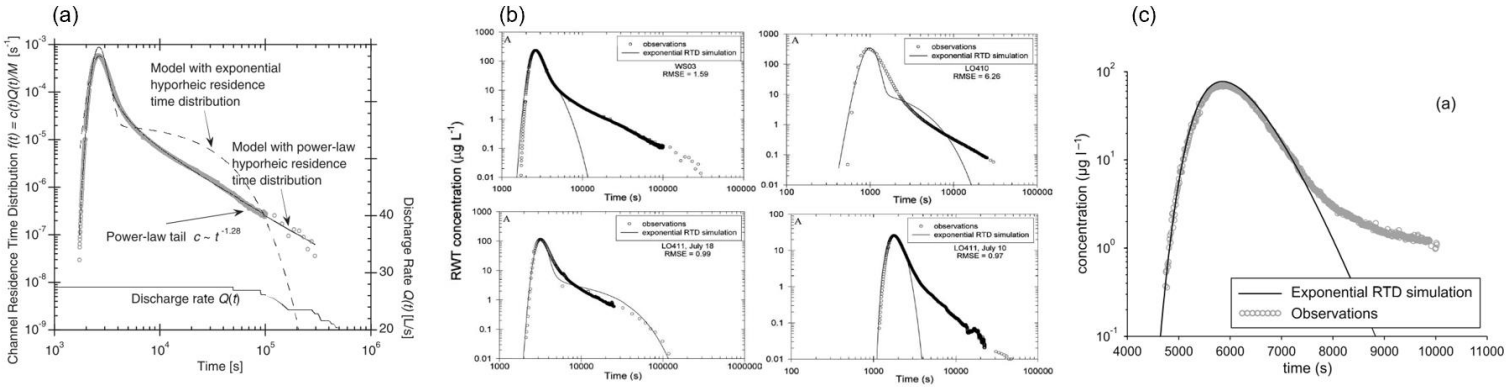


Figure 8. Simulation results from previous studies (a) Haggerty et al. (2002) (b) Gooseff et al. (2003) (c) Marion et al. (2008)

In this respect, several parametric equations for the retention time distribution have been proposed with particular mathematical forms, such as lognormal, power law, or gamma function (Cardenas, 2007; Drummond et al., 2017; Haggerty et al., 2002; Stonedahl et al., 2012; Wörman et al., 2002; Wörman and Wachniew, 2007). Elliott & Brooks (1997) and Elliott et al. (1997) studied the physical process of mass exchange with the hyporheic zone, and suggested the formula of retention time function with hyporheic properties. Marion & Zaramella (2005) and Marion et al. (2008) presented the combination of the exponential behavior of TMS and the function by Elliott & Brooks (1997) to improve simulation accuracy. Although those models employed different approaches, their objectives were to find the optimal mathematical formula of the retention time distribution, and to validate the accuracy by comparing its simulation result to BTCs curves measured at the flow zone.

However, since the storage effect is less responsible for solute mixing than flow dynamics, errors of retention time modeling may not be revealed through the BTCs obtained in the surface flow zone. Hence the retention time function modeling should be validated with the actual solute behavior within storage zones. For this reason, several studies (Gooseff et al., 2011; Jackson et al., 2012; Mignot et al., 2017; Sandoval et al., 2019; Weitbrecht et al., 2008) implemented in-storage zone measurements under the restricted experimental conditions, or in a few visible surface storage zones of streams, due to the diversity, invisibility, and unclear boundary of natural storage zones. Unfortunately, those studies were very limited in

terms of spatial scale to represent the overall heterogeneous storage zones of natural rivers.

## 2.3 Determination of TSM parameters

Modeling of solute mixing cannot be based on fixed parameters, but must provide for a simulation over representative time and length scale of simulation including spatio-temporally varying parameters. The 1D solute transport models roughly characterize the complex streamflow and heterogeneous topography of the river with only several parameters. For example, the simulation of the 1D ADE requires determination of river velocity and longitudinal dispersion coefficient. The TSM characterizes the storage effect with two additional parameters: relative size of storage zone and mass exchange rate between the storage zone and the main flow zone. The methods for TSM parameter determination are classified in Figure 9. Unfortunately, even for decades of TSM, there have not been clear understanding of meaningful approximation of the parameters for physical process. They are not additive across increasing distance (Gooseff et al., 2013) and it has no pattern with discharge (Ward et al., 2013; Zarnetske et al., 2007). Even though several theoretical and empirical estimates for these parameters have been proposed for recent decades (Cheong et al., 2007; Cheong and Seo, 2003; Femeena et al., 2019; Noh et al., 2021; Pederson, 1977; Rowiński et al., 2005; Rowiński and Piotrowski, 2008; Sahay, 2012; Thackston and Schnelle, 1970), it has been reported that the theoretical estimates

still have an inaccuracy due to their assumptions while the empirical estimates still have data dependence. Accordingly, the parameter determination still predominantly relies on optimization techniques. Such optimized parameters, however, are products of various uncertainties from the over-simplification of the 1D approach, numerical setting for optimization such as grid size or objective function (Noh et al., 2021, 2019; Wallis and Manson, 2019), equifinality problem (Choi et al 2020), and measured data itself. Consequently, the 1D models has poor applicability due to the difficulty in determining representable parameters which is yet to clearly resolved. Now, we cast doubt on if the processes estimated from conceptualization of TSM are actually interpretable.

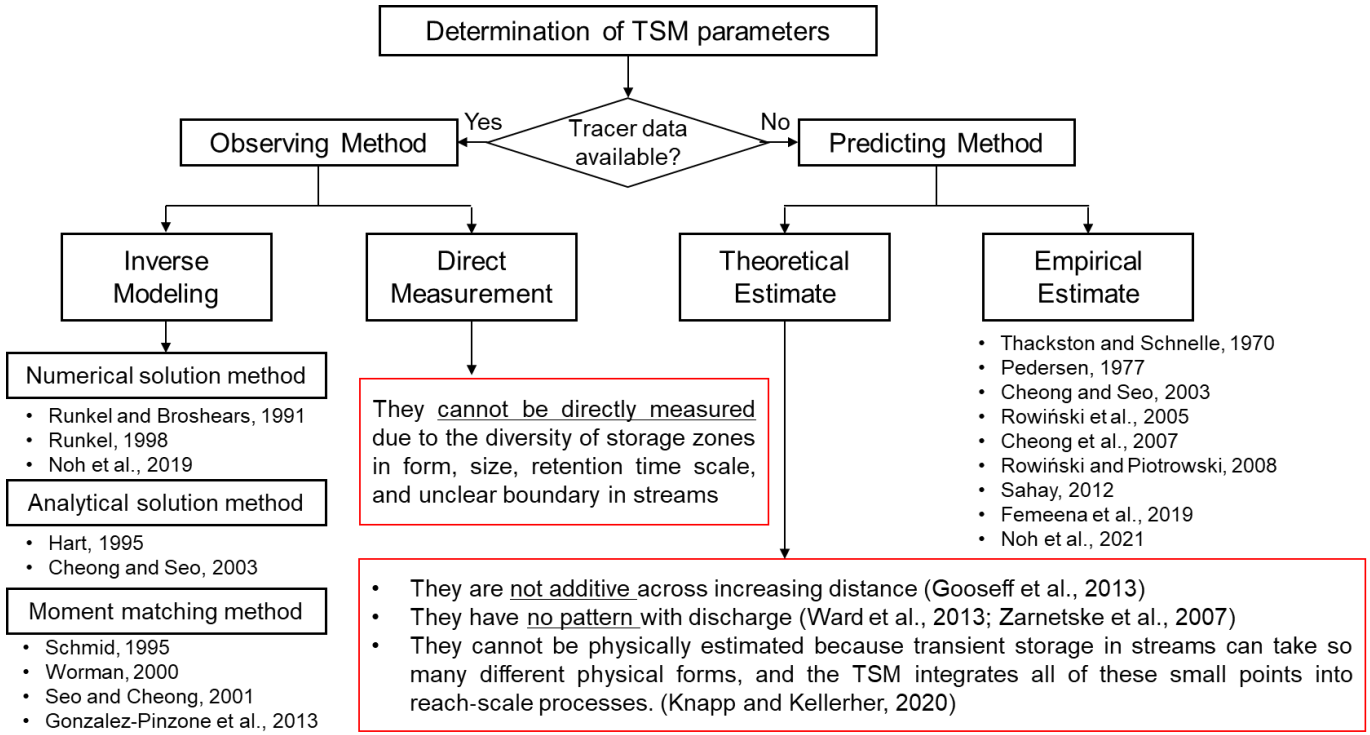


Figure 9. Classification of determination of TSM parameters.

## 2.4 Summary of literature review

From “Theoretical Background”, it is remarkable that even for last decades of TSM conceptualization, we still lack of clear understanding of physical interpretation of TSM parameters, in turn the parameter determination still relies on the inverse modeling from observation. Then, the validity of TSM simulation is highly dependent on the reliability of the observation. Unfortunately, the storage effect of irregular and heterogeneous streams is difficult to be observed and quantified. Consequently, the BTCs observed at surface flow are still used for the validation of TSM and other conceptual models. However, the BTCs are less sensitive on the storage effect than the flow dynamics. Therefore, there is a need of the reliable data that can independently represent the in-stream storage effect.

Hence, the goal of this research are to develop and verify an method capable of quantitatively estimating the effect of the storage zone from BTC observations at flow zone. The detailed objectives are:

1. Developing an explicit equation to distinguish the effects of flow dynamics and storage zones, and estimating the storage effect of streams using signal deconvolution in Fourier domain. (50%)
2. Evaluating the accuracy of TSM simulation and corresponding parameters comparing to the storage effect estimation. (30%)
3. Predicting biodegradation rate of organic chemicals flowing along a stream using the estimated retention time. (20%)

# CHAPTER III

# MATERIALS AND METHODS

## 3.1 Tracer experiments in a stream

### 3.1.1 Site description

The spatial–temporal concentration variation of tracer in a stream involves the information of both flow dynamics and complex storage effects of the stream. To acquire such information, the tracer test was carried out at the 4.85 km reach of Gam Creek, South Korea, in October 2019. The testbed of Gam Creek is a sand-bed braided stream, and has potential storage zones, such as shoals, dunes, side pockets, and natural banks (see Figure 10 & 11). The well-known tracer material, Rhodamine WT (RWT), was used due to its visibility and detectability. Runkel (2015) stressed the significance of considerable sorbability of RWT, especially for groundwater & hyporheic tracer studies. Based on his arguments, its application in this study is justified for two reasons: First, this study is designed to kinematically investigate residence time regardless of mass or concentration. Payn et al. (2008) and Aubeneau et al. (2015) revealed that sorption reactions hardly change the fundamental shape of breakthrough curves; hence the sorbability of the RWT may not affect the residence time distribution. Second, even though the storage effect plays a significant role in forming breakthrough curve tails, the NRTF is determined by not only the tail, but also the bulk of the tracer profile. Portions of the breakthrough curve prior to the tail represent the tracer that has been transported by the advective flow, and thus less affected by sorption (Runkel, 2015).

As a result, neglecting the RWT sorbability to investigate the residence time in streams is acceptable.

The first measurement station (S1) should be located far enough from the injection point (IP), in that the tracer should be completely mixed in the transversal and vertical directions for one-dimensional analysis. The required distance can be estimated using equation (12) (Kilpatrick & Wilson, 1989):

$$L_0 = 0.1\left(\frac{1}{n}\right)^2 \frac{UW}{E_z} \tag{16}$$

where $L_0$ is the distance required for complete mixing, n is the number of injection points, W is a mean top width, and $E_z$ is a lateral mixing coefficient, which is estimated by $E_z/Hu_* = 0.15$ (Fischer et al., 1979). In this testbed, the estimated $L_0$ was 411.61 m which was smaller than the distance of S1 from the injection point of 820 m.

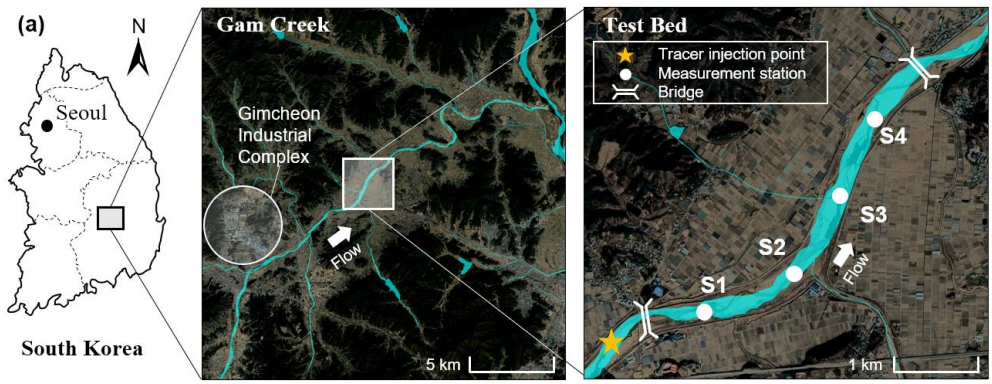


Figure 10. Site map and locations of in-stream measurement stations for the tracer tests conducted at the Gam Creek, South Korea

Figure 11. Braided flow shape in S3-S4 section, Gam Creek in 2019

### 3.1.2 Tracer Measurement

The concentration of RWT was measured using YSI-600OMS fluorometer at measurement stations downstream. The fluorometers were calibrated beforehand in the range of 0 to 200 ppb with a standard RWT solution. The measurement error range of the fluorometer was ±5 % of the reading values or 1 ppb, and the sampling rate was 0.25 Hz. Three or four fluorometers were uniformly installed at the measurement stations equally spaced and collinear in transverse direction at each measurement station (S1–S4 in Figure 10) for cross-sectional average concentration. Table 3 summarizes the hydraulic and geometric properties of the test reach of the Gam Creek. The discharge and velocity profiles were measured by acoustic Doppler current profiler (ADCP RiverSurveyor S5). The reach length, mean depth, mean width, and channel slope were measured by Real-Time Kinematic-Global Positioning System (RTK-GPS Sokkia GRX1). In addition, the tracer cloud was monitored by an RGB camera mounted on a drone (DJI Mavic 2). This bifurcated tracer cloud shape was observed in the measured breakthrough curve, as well as in the moving tracer cloud.

Table 3. The hydraulic and geometric conditions of the tracer test.

| Sub-Reach | $Q$ $(m^3s^{-1})$ | $RL$ $(m)$ | $H$ $(m)$ | $W$ $(m)$ | $U$ $(ms^{-1})$ | $S^{(1)}$ $(-)$ | $S_n^{(2)}$ $(-)$ |
|---|---|---|---|---|---|---|---|
| Reach 1 (S1-S2) | 12.82 | 1,200 | 0.361 | 57.4 | 0.668 | 0.000825 | 1.07 |
| Reach 2 (S2-S3) | 12.91 | 830 | 0.358 | 58.9 | 0.665 | 0.000825 | 1.03 |
| Reach 3 (S3-S4) | 12.84 | 2,000 | 0.431 | 53.0 | 0.681 | 0.000825 | 1.08 |

(1)Mean bed slope (2)Sinuosity which is a ratio of the curvilinear length to the straight-line length between the ends of the sub-reach

### 3.1.3 Preprocessing for Breakthrough Curves

The tracer test is a long-standing technique to indirectly identify the streamflow dynamics. Early tracer tests were able to provide only a few of concentration data by sampling to form a BTC due to lack of measurement technique (measuring once in minutes, hours, or even days) (Cox et al., 2003; De Smedt et al., 2005; Drummond et al., 2017, 2014; Gooseff et al., 2013; Piotrowski et al., 2007; Runkel, 1998). As the tracer measurement technique have been advanced recently, it is possible to acquire numerous data for a single BTC (measuring once in seconds) (Baek et al., 2019; Bottacin-Busolin et al., 2011; Kim et al., 2021b; Shin et al., 2020). This advancement enables us to investigate smaller time-scale behavior of tracer transport along a river, but unfortunately it accompanies undesired noise as well. Due to the irregularity and randomness of nature, such as turbulence or morphological irregularity, the scale of such noise from rivers is much larger than common noise of digital signal. Therefore, the tracer BTC from rivers require more intensive denoising

techniques to clarify its mean behavior. However, the denoising process always distort the original information of primary data so that care must be taken.

Before BTC denoising, truncation of background concentration has to precede on raw data. It is challenging to separate the BTC range from background concentration without information loss, especially in the tail part due to the error range of the fluorometer. The improper tail truncation could negatively affect mass-related or storage zone-related analysis (Drummond et al., 2012). From experimental studies, several researches found that the late-time behavior of BTCs has a power-law residence time distribution (RTD) in storage zone (Gooseff et al., 2005; Haggerty et al., 2002; Schumer et al., 2003). This tendency in BTC tail can lead the criteria of truncation point. Therefore, in this study, based on the power-law RTD assumption, the BTCs were plotted in log-log space, and the tailing part was truncated at the point where the linear relationship ends. The total mass of truncated BTCs was then recovered using the known injected mass of RWT to supplement the conservative tracer assumption. As argued in previous studies, the mass recovery rate of RWT is relatively low due to its sorbability (Runkel, 2015). However, Payn *et al.* (2008) and Aubeneau *et al.* (2015) have reported that sorption process do not change the fundamental shape of BTC. In this study, the average mass recovery rate of all experiments in this study was estimated as 84%, which is relatively higher than those that were summarized in Runkel (2015).

3.2 Development of algorithm for storage effect quantification

### 3.2.1 Concept of residence time distribution

When a number $N$ of solute particles was instantaneously introduced into a reactor, they may not release out simultaneously. The residence time within the reactor is different in different particles. The number of particles of the $N$ released within a time interval is the probability of the particles' residence time in the time interval. Accordingly, the residence time distribution can be plotted as probability density function (PDF). This concept can not be only applied for the number of particles, but also for mass or concentration.

The one-dimensional solute transport modeling is founded on the tracer test data. However, the downstream breakthrough curve from tracer test cannot frequently preserve the initial mass at the upstream boundary. Thus, the mass is often artificially recovered or the loss is lumpedly represented by first-order decay term. This in turn, indicates that the concentration data is not reliable. Therefore, in this study, the observed breakthrough curves are converted to the residence time distribution to kinematically analyze the temporal behavior of tracer regardless of mass

### 3.2.2 Convolutional Decomposition Equation (CDE)

The propagation of solute released into a riverine system is referred as to non-Fickian transport because it is not only dominated by Fickian behavior but also by surrounded storage zones. To identify the effect that causes non-Fickian transport, we decomposed the Fickian behavior in surface flow and retention effect of storage zones.

A time it takes particles travel in streams $T$ can be divided into two: a time that particles move $T_m$ and a time that particle be stopped $T_s$ ($T = T_m + T_s$). The flowing surface water induces the particles to move downstream whereas inherent storage zones of channel restrict their mobility. Accordingly, the measured temporal data at surface water is a result from such combined system. The time variables for surface flow indicate how much time particles travels along the surface flow, and thus it is referred as to the residence time. Since the probability of certain residence time interval for a distance can be expressed as the portion of solute travels the distance for that time interval, the probability density function of residence time (also referred as to residence time distribution) can be easily related from the concentration data:

$$r(t;x) = \frac{C(t;x)}{\int C(t;x)dt} = \frac{M}{Q(t)}C(t;x) \tag{17}$$

where $r$ is the residence time distribution, $C$ is the time-concentration data at a streamwise distance $x$, $Q$ is a flow discharge, and $M$ is a total mass of solute introduced in a stream.

The solute behavior in a surface flow without channel-morphological consideration is commonly interpreted as the Brownian motion with drift. However, this ideal behavior has a discrepancy in actual system due to the storage effects. The residence time distribution for this non-Fickian transport can be expressed with convolution operation with those for Fickian transport and storage effect.

$$r_{nF}(t;x) = r_F(t;x) * \Phi(t) = \int_0^t r_F(\tau;x)\Phi(\tau - t)d\tau \tag{18}$$

where the asterisk symbol denotes the convolution operator, $r_F$ and $r_{nF}$ is the residence time distribution for Fickian transport and non-Fickian transport, respectively, $\Phi$ is the Net Retention Time Function (NRTF), and the $\tau$ is dummy time variable. If there is no affection of the storage effect in riverine domain (in rare cases), the $\Phi$ has a form of the Dirac delta function as

$$\Phi(t) = \begin{cases} 1, & at\ t = 0 \\ 0, & at\ t > 0 \end{cases} \tag{19}$$

It must be noted that the $r(t)$ is on the Eulerian time domain that focuses on specific time range. Whereas, the $\Phi$ is on the Lagrangian time domain that $t = 0$ indicates that particles does not stay in a storage zone.

The ADE is a classical model for the Fickian transport of a particle in streams. As previously mentioned, the shapes of residence time distribution in surface flow is equivalent to those of concentration-time curve in the same domain. Accordingly, the relevant residence time distribution can be inferred from the governing equation of the ADE.

$$\frac{\partial r_F(t;x)}{\partial t} + u\frac{\partial r_F(t;x)}{\partial x} = D_L\frac{\partial r_F(t;x)}{\partial x} \tag{20}$$

where $u(m/sec)$ is a reach-averaged flow velocity, and $D_L(m^2/sec)$ is a longitudinal dispersion coefficient. When a mass pulse is instantaneously released at the upstream boundary, and $C(x \to \infty, t) = C(x, t = 0) = 0$, the solution of Eq. (20) can be inferred from the analytical solution of the ADE.

$$r_{nF}(t;x) = \int_0^t \left[\frac{x}{\sqrt{4\pi D_L \tau^3}}\exp\left\{-\frac{(x-u\tau)^2}{4D_L\tau}\right\}\right]\Phi(\tau - t)d\tau \tag{21}$$

Eq. (16) is advantageous for fast computation and less risk of error due to the deterministic calculation, but it has the shortage from the limited configuration of the upstream boundary condition. Such instantaneous injection, as shown in Figure 12a, is experimentally difficult to fulfil, and even if the multi-point injection (or line injection) were performed, the tracer may appear to be a three-dimensional behavior. It should be noted that the one-dimensional analysis is only allowed after when the transversal and vertical mixing of solute along the stream is completed. The location of the upstream boundary should be far enough from the injection, more than the Taylor's initial period, so that the transversal and vertical mixing is complete, as shown in Figure 12b. Thus, the mass pulse injection is not experimentally feasible.

Alternatively, the analytical solution in which the shape-free breakthrough curve can be applied as an upstream boundary condition were developed using the concept of *routing procedure* (Fischer, 1966; Fischer, 1968; Baek and Seo, 2010; Baek and Seo, 2020; Baek, 2021). The *routing procedure* was initially developed in order to estimate the dispersion coefficient from two concentration-time curves measured at different stations. In other words, we can expect a downstream curve if a upstream curve and a dispersion coefficient are known. This 1D routing model requires the underlying assumption that no dispersion occurs during the solute cloud passes the measuring point, referred as to the *frozen cloud approximation*. Using the routing model, the analytical solution for Eq. (15) can be yielded as

$$r_{nF}(t;x) = \int_0^t \int_0^{\tau_2} \left[ \frac{r_{nF}(\tau_1;0)u}{\sqrt{4\pi D_L T_c}} \exp\left\{ \frac{\{x-(\tau_2-\tau_1)U\}^2}{4D_L T_c} \right\} \right] \Phi(t-\tau_2) d\tau_1 d\tau_2 \quad (22)$$

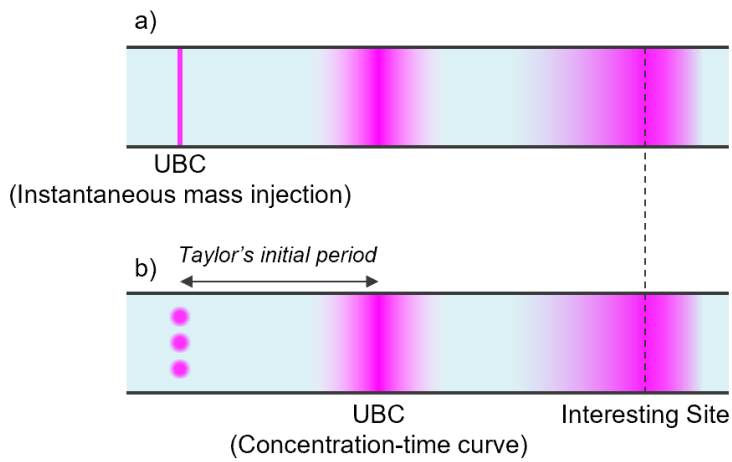


Figure 12. Schematics of difference of upstream boundary conditions (a) Instantaneous mass pulse (Dirac delta function) (b) Concentration-time distribution

### 3.2.3 Deconvolution technique with BTCs

In this study, a breakthrough curve was deemed an impulse-response signal, and we applied the deconvolution technique to estimated the $\Phi$ from tracer breakthrough curves. Deconvolution is a useful technique in various fields to identify submerged information within a measured data by subtracting known components. For example, in digital image processing, the deconvolution technique is often used to restore the original sharp image from a blurred image (Krishnan and Fergus, 2009; Kundur and Hatzinakos, 1996). Such deconvolution, also known as inverse calculation, has also been used a few times with breakthrough curves from streams. Payn et al. (2008) calculated the non-parametric residence time distribution of solute at the reach scale using concentration curves measured at up- and downstream boundaries. They described the difficulty of deconvolution in the frequency domain because of the high frequency variability, and applied an alternative method, Geostatistical inversion. Another approach, maximum entropy deconvolution, was also used to investigate solute transport (Guymer & Stovin, 2011; Hart et al., 2016; Sonnenwald et al., 2011, 2014, 2015). Gooseff et al. (2011) attempted to estimate the memory function and proposed the validity of the Wiener filtering method for high-frequency noise cancellation. However, undesired oscillating distortion was seen in their results, which is known as the Gibbs phenomenon (Gibbs, 1898). This physically irrelevant phenomenon can often be observed in the filtering process and reduces the reliability of the results. To overcome such difficulties in the deconvolution process, we proposed the data stabilization method as below.

Breakthrough curves from nature contain considerable unexpected noise, which might be noise from Brownian motion, or fluctuations due to intricate unknowns, such as turbulence. So far, existing macroscopic studies for breakthrough curve have not required the investigation of these small time-scale variabilities. However, the deconvolution technique is a mathematical operation of the breakthrough curve in the Fourier domain, and thus such instability can induce serious computational errors.

The convolution operator of equation (2) is converted to the multiplication in the Fourier domain as below:

$$\widetilde{r_{nF}}(i\omega; x) = \widetilde{r_F}(i\omega; x) \times \widetilde{\Phi}(i\omega) \tag{23}$$

where, upper tilde denotes a function converted from the time domain into the frequency domain by the Fast Fourier Transform (FFT). This was performed via an algorithm in Python language. For temporally equally spaced finite discrete series of both the experimental concentration data and simulation results, the discrete approximation of the FFT was derived as below (Bendat and Piersol, 2000):

$$\tilde{x}(\omega) \triangleq \sum_{n=0}^{N-1} x_n e^{-i2\pi\omega n\Delta t} \tag{24}$$

where $x_n$ is the $n$th data among what is sampled at $N$ equally spaced points an interval $\Delta t$ apart, $i$ is the imaginary number $\sqrt{-1}$, and $\omega$ is the discrete frequency defined as $\omega = k/(N\Delta t)$ $(k = 1, 2, \dots, N-1)$.

In equation (15), $\Phi$ can be obtained by dividing $\widetilde{r_{nF}}$ by $\widetilde{r_F}$, and then inversely converting to the temporal domain. In such deconvolution process, care must be taken due to the noise amplification problem. Figure 8a shows the raw data of $\widetilde{r_{nF}}$ measured at S2 of the tracer test, and the corresponding simulation result of $\widetilde{r_F}$ by the Routing model plotted in the frequency domain. These two show periodic distributions, with different amplitude and similar wavelength in the low-frequency band. In this region, the deconvolution can function as an operator of dividing the amplitude values. However, above a certain frequency, ~0.005 Hz in Figure 13, wavelengths of $\widetilde{r_{nF}}$ and $\widetilde{r_F}$ are likely to be significantly different. If at any frequency the numerator $\widetilde{r_{nF}}$ increases and the denominator $\widetilde{r_F}$ decreases close to zero, $\widetilde{\Phi}$ increases to infinity, and *vice versa*. These phenomenon in the deconvolution process are known as poles and zeros. If a function has at least one pole, then the system is unstable (Bendat and Piersol, 2000). From the deconvolution in Reach 1 of the tracer test, the poles grow to the order of $10^{14}$ in the higher band, as shown in Figure 13b, and this unstable data cannot shape any ordered distribution in the time domain. Payn et al. (2008) also stated that the high-frequency variability makes the time domain distribution impossible to interpret.

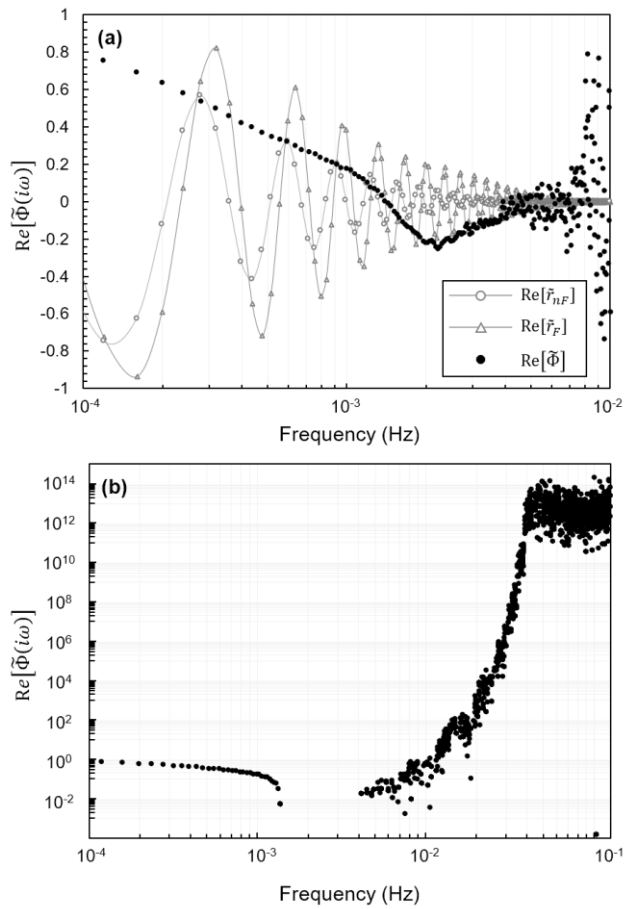


Figure 13. Components of equation (15) in the frequency domain estimated from measurements at S2 of the tracer test in which the NRTF was calculated by $\widetilde{\Phi} = \tilde{r}_{nF}/\tilde{r}_F$ (real part only). (a) Semilog plot bounded by $\left|\mathrm{Re}\left[\widetilde{\Phi}\right]\right| < 1$ and $10^{-4} < \omega < 10^{-2}$ (b) Log-log plot bounded by $\mathrm{Re}\left[\widetilde{\Phi}\right] > 0$ and $10^{-4} < \omega < 0.125$, in which the 0.125 Hz is the Nyquist frequency of the dataset.

### 3.2.4 Data stabilization for deconvolution

Since the aim of the deconvolution in this study is to identify the significant range of the net retention time, such high-frequency variability is not in consideration. Accordingly, we applied a low-pass filter to restrain the divergence. In the filtering process, two strict conditions must be satisfied: First, as the purpose of filtering, the filter kernel should be able to effectively block the high-frequency contributions, so that the temporal data sequence should disclose its mean behavior. Second, the filtering process always distorts the primary data, and thus it must be ensured that the degree of distortion is acceptable. A common approach for the filtering is to design a Frequency Response Function (FRF), which is the ratio of the amplitudes of the modified data sequence to those of the given data sequence (Duchon, 1979). Among the FRFs, that of the ideal low-pass filter preserves the prior band of cutoff frequency, and completely rejects the latter band; its frequency response is a rectangular function (see Fig. 14). This was realized mathematically by multiplying a signal by the rectangular function in the frequency domain. However, a modified data sequence with such steep roll-off would exhibit undesirable oscillating artifacts, called the Gibbs phenomenon (Duchon, 1979). The Gibbs phenomenon is frequently manifested by such simple truncation, and in turn negatively affects the convergency of the Fourier transform and computation speed (Chen and Sivan, 2021). Accordingly, restraint of the Gibbs phenomenon is the additional required condition for filtering. The Butterworth filter was employed as an alternative for piecewise smooth transition, and its FRF is given by

$$|H(i\omega)| = \frac{1}{1 + \left(\frac{\omega}{\omega_c}\right)^{2N}} \tag{25}$$

where $|H(i\omega)|$ denotes the FRF of the Butterworth filter, and $N$ denotes a filtering order that configures the transition smoothness. In this problem, the contribution of the high band is too high not to be sufficiently blocked with a smoothed transition. Therefore, we designed the filter in which the lower band than the cutoff frequency was smoothed by the Butterworth filter, and higher band than the cutoff frequency was completely stopped, as shown in Figure 14.

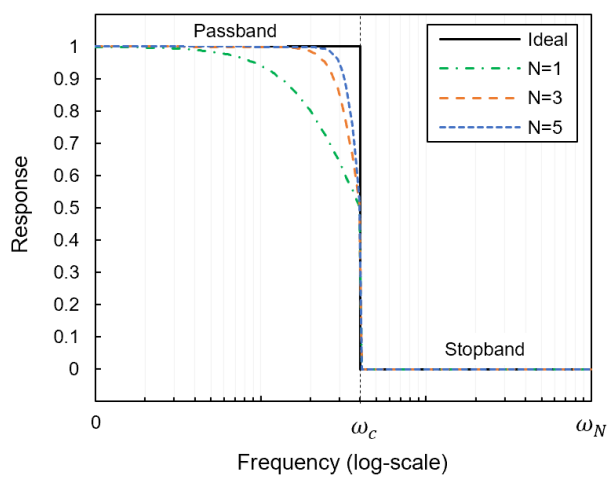


Figure 14. Transition shapes of the ideal filter and the Butterworth filter by varying

filtering order.

The key to the filtering is to determine the parameters: the filtering order, and the cutoff frequency. As the filtering order increases, the Gibbs phenomenon can be reduced, while the modified data sequence in the time domain tends to be scattered. Such tendency violates the first condition previously mentioned. As the order decreases, certain shapes of distribution in the time domain can be revealed, but undesired oscillation could be evident as well, as was seen in the results of Gooseff et al. (2011). To effectively eliminate the poles, the cutoff frequency should be low enough. However, if it is too low, the information of the primary data can be distorted, and the original residence time distribution may collapse. The most vulnerable part to the collapse is the peak value, and Figure 15 plots the peak collapse rate according to the cutoff frequency at each case of the tracer test. Based on the acceptable peak collapsed rate, the proper cutoff frequency was determined by equation (18):

$$\omega_c = \underset{\omega_c \in [0,\omega_N]}{\arg\min} \left| \left| \frac{\max_{t\in T} r_{obs.} - \max_{t\in T} \mathrm{F}(r_{raw}; N, \omega_c)}{\max_{t\in T} r_{obs.}} \right| - \varepsilon_a \right| \tag{26}$$

where F(·) denote the filtering operator with the order, $N$, and the filter cutoff frequency, $\omega_c$(Hz), $\omega_N$ is the Nyquist frequency that is one-half of the sampling

rate, and $\varepsilon_a$ is the allowed error rate configured as 0.01 in this study, indicating 99 % of the peak information is preserved.

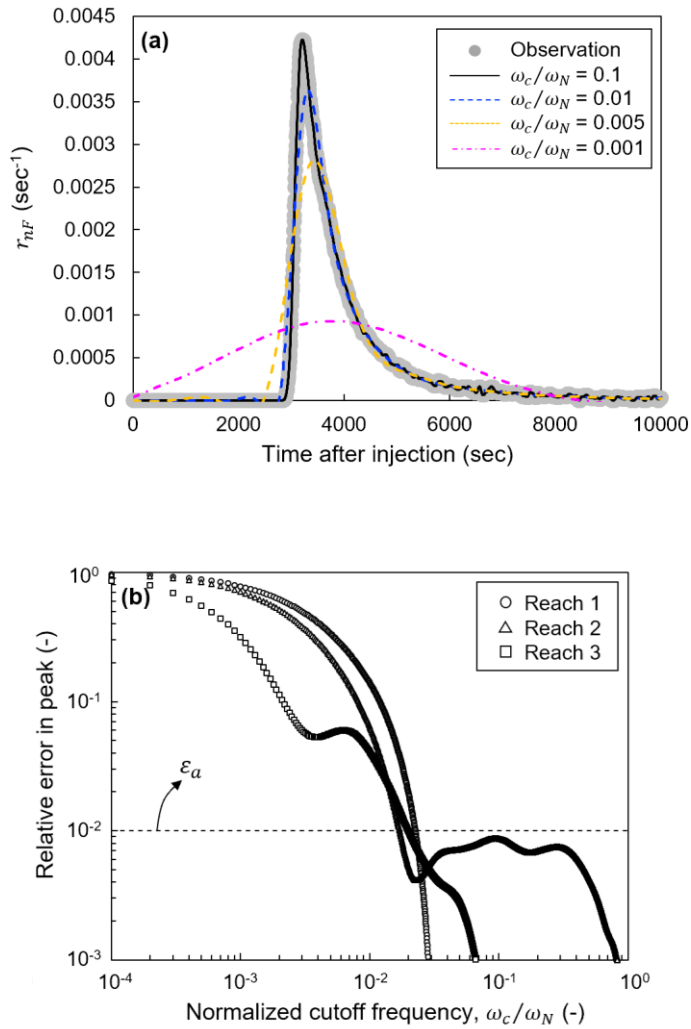


Figure 15. Peak collapse aspect according to cutoff frequency (a) breakthrough curve variation in Reach 1 (N=3) (b) Relative errors in peak values

### 3.2.5 Parameter estimation

The $r_F$ contains two unknown parameters; mean flow velocity and longitudinal dispersion coefficient, which represents flow properties of surface flow. The method is twofold to determine the mean velocity for each sub-reach: One is to use arithmetic mean of the measured velocity data at the ends of the sub-reach, and the other is to use the measured concentration data. During the tracer tests, the measured velocity was cross-sectional averaged, not reach-averaged. The velocity-based method thus requires an additional assumption that the flow velocity varies linearly in streamwise direction. Whereas the concentration-based method is to use concentration change which is affected by actual flow characteristics of sub-reach, including flow irregularities such as turbulence. Therefore, due to the better representability, the concentration-based method was applied in this study.

The longitudinal dispersion coefficient is a key of solute transport modeling because it is directly connected to dilution mechanism and is difficult to be accurately estimated. The determination methods for the dispersion coefficient can be divided into two; theoretical models and empirical models, and inverse modeling. The theoretical models are relatively early models considering dispersion induced by special velocity gradient and corresponding shear flow (Elder, 1959; Fischer, 1975, Fischer et al., 1975). However, since solute mixing in streams is not only from the shear flow, but also from other complicated factors, such theoretical approach has yielded practically poor accuracy. On that account, the various empirical

estimates have been proposed which treat the dispersion coefficient as a function of measurable data such as hydraulic flow properties and channel morphology based on the intensive indoor and field experiments; resultingly they have shown better accuracy.

However, the goal of the CDE model is to decompose the mixing processes in the surface flow and the storage zone. Accordingly, the longitudinal dispersion coefficient unaffected by the storage effect is required in the model, and thus we brought back the theoretical models. Marion et al. (2008) demonstrated the relevance of the Fischer's formula (Fischer, 1975, Fischer et al., 1975).

$$D_L = 0.011 \frac{u^2 W^2}{u_* h} \tag{27}$$

However, since the equation is a semi-empirical due to the constant value determined based on relatively small-scale experimental data and the $D_L$ is a function of the width to the power of 2, the $D_L$ can be over-estimated when the width of subject channel is large. Considering the average width of 56.43 m in case of the GC2019, the Fischer's formula cannot be applied. Therefore, we employed the Elder's equation which is for mixing in-plane boundary layer flow with infinite width.

$$D_L = 5.93hu_* \tag{28}$$

The parameters $T_h$ and $\alpha_h$ included in the $r_r$ were estimated from the measured concentration data. The parameters of which yielded minimum errors in comparision between the simulation concentration and the observed concentration. As an objective function for the comparision, the Route Mean Squared Error (RMSE) is used, defined as

$$\text{RMSE} = \sqrt{\sum_{j=1}^{N_{obs}} \frac{\left(r_{obs}^{j} - r_{sim}^{j}\right)^2}{N_{obs}}} \tag{29}$$

where the $C_{obs}^{j}$ is the observed residence time data at $j^{\text{th}}$ time step, the $C_{sim}^{j}$ is the simulated residence time data at $j^{\text{th}}$ time step, and the $N_{obs}$ is the number of observation data.

For such optimization technique, we should beware the failure of finding the global optima. In parameterization of nature system, there are often a single global optimum and multiple local optima with multiple parameter combinations. In such non-convex problem, the optimized parameters easily sink into the local optima, and may be differently obtained in different initial guess or bounds. In this case, the global optimization techniques are required which are computationally costlier.

This being so, we evaluated the convexity of the model structure by plotting the minimum RSME variation depending on varying $T_h$ and $\alpha$. As seen in Fig 14, for all the sub-reaches, the overall RSME gradients seem to be convex. Even though Figure 14 shows a small plateau near the 0.001 $sec^{-1}$ of $\alpha$ and Figure 16 is likely to shows multiple optima, they are induced by the fluctuation of the measured concentration data and their RSME differences are minor. On this basis, to solve the error minimization problem, we used the SLSQP (Sequential Least Squares Programming) which is a simple optimization scheme using the quasi-Newton method (Kraft, 1988).

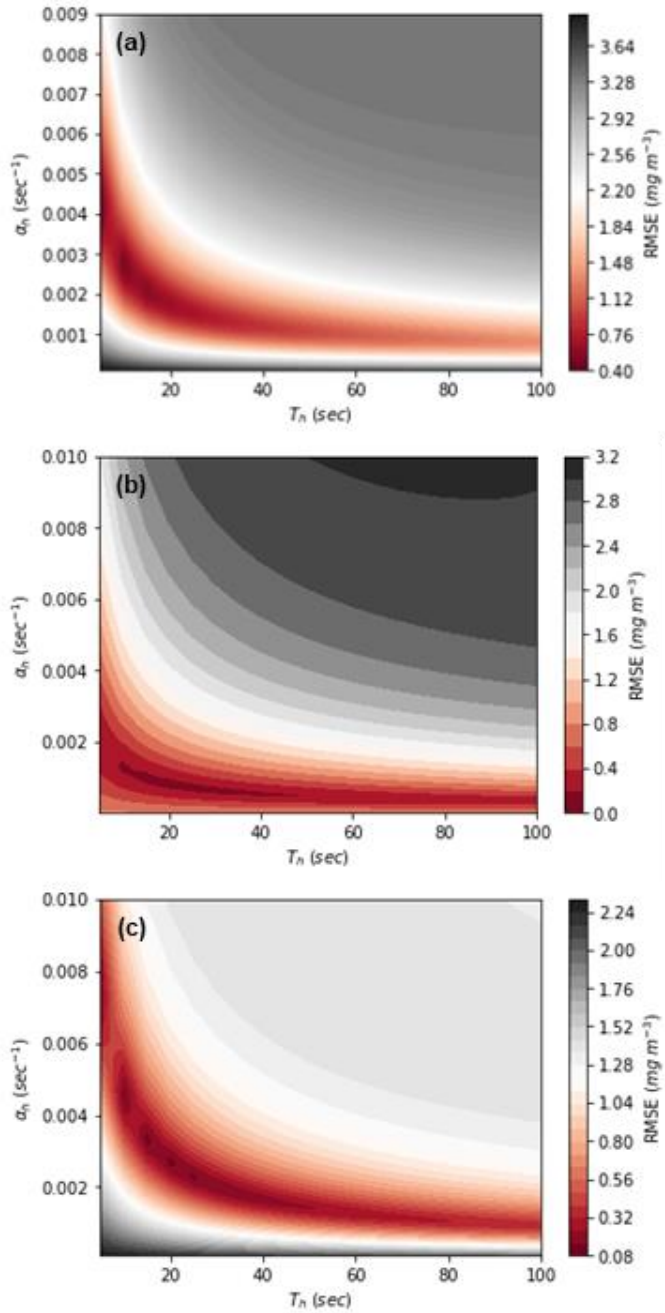


Figure 16. 2D Contour plots from 3 lists: $T_h(\epsilon/\alpha)$, $\alpha$, and resulting RSME

3.3 Net retention time distribution in TSM

If solute with a time-concentration curve $C$ in surface flow was transiently trapped once in a lump into a storage zone and released back to surface flow after a retention time distribution $\varphi$, its primary $C$ is lagged affected by the storage zone as much as the $\varphi$ and turns to $C * \varphi$. Accordingly, the $\varphi$ represents the inherent storage effect of the stream and it may different in different streams. Non-Fickian models often includes a sink-source term into the ADE. As well as the TSM, the sink-source rate is proportional to the concentration difference. Using the defined $\varphi$, the non-Fickian model can be expressed as below.

$$\frac{\partial C}{\partial t} = \left(-u + D_L \frac{\partial}{\partial x}\right)\frac{\partial C}{\partial x} + \alpha(C - C * \varphi) \tag{30}$$

where $u(m\, s^{-1})$ is mean flow velocity, $D_L(m^2\, s)$ is longitudinal dispersion coefficient, and $\alpha(s^{-1})$ is mass exchange rate. Eq. (18) can be written in the Laplace domain as

$$\left[s + \alpha\left(1 - \bar{\varphi}(s)\right)\right]\bar{C}(s;x) + U\frac{\partial}{\partial x}\bar{C}(s;x) - D_L\frac{\partial^2}{\partial x^2}\bar{C}(s;x) = \bar{C}(t=0) \tag{31}$$

where the upper bar denotes variables in Laplace domain, and $s$ denotes a Laplace variable. Meanwhile, the governing equation of the TSM were given as

$$\left[s+\alpha\left(1-\frac{\frac{\alpha}{\epsilon}}{\frac{\alpha}{\epsilon}+s}\right)\right]\bar{C}(s;x)+U\frac{\partial}{\partial x}\bar{C}(s;x)-D_L\frac{\partial^2}{\partial x^2}\bar{C}(s;x) = \bar{C}(t=0) \tag{32}$$

where $\epsilon$ is the relative volumetric size of the storage zone to the flow zone. As a result, substituting the exponential distribution with the parameter $\alpha/\epsilon$ into the $\varphi$, Eq. (19) becomes equivalent to the governing equation of the TSM. Two different solutions were compared in Table 4.

Under the assumption that the storage zones are homogeneous and uniformly distributed along the reach (see Fig. 17), Marion et al. (2008) proposed the exact solution for $\Phi(\mathrm{t})$ with a stochastic approach. Following their derivation, the defined NRTF can be expressed as below:

$$\Phi(\mathrm{t})=\sum_{n=0}^{\infty}\left\{\frac{(\alpha T_c)^n e^{-\alpha T_c}}{n!}\right\}\{\varphi(t-\tau)\}^{*n} \tag{33}$$

where $T_c$ is characteristic time defined as $x/u$. To sum, the NRTF can be mathematically defined with the mass exchange rate $\alpha$ and the retention time distribution $\varphi$. Furthermore, the NRTF for the TSM can be inferred using the exponential form of the $\varphi$.

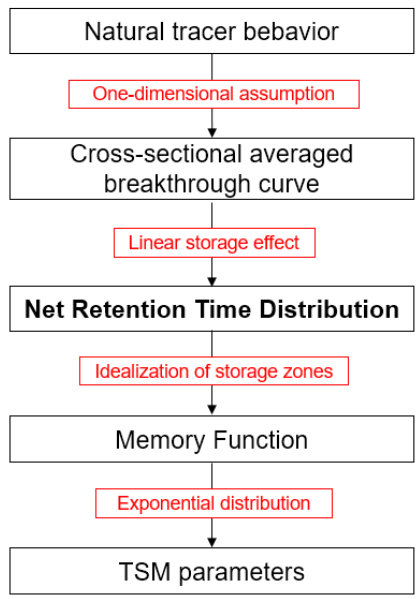


Figure 17. Phased assumptions for TSM modeling

Table 4. Comparison between TSM parameters and NRTD in storage effect quantification

| | **In storage effect quantification** | |
|---|---|---|
| | **TSM parameters** | **NRTD** |
| Parameter | 2 parameters ($\alpha$, $\epsilon$) | Non-parametric distribution |
| Assumption | Linear storage effect<br>Ideal storage zones<br>Exponential memory function | Linear storage effect |

| Estimation | Optimization | Deconvolution |
|---|---|---|
| Pros | Simplicity & Applicability<br>Low computational cost<br>Existing relevant studies | Closer to actual storage effect |
| Cons | Over-simplification<br>Equivocal physical meaning | Difficulty in estimation due to high-frequency variability of data |

Additionally, we compared the simulation results of the TSM and the CED with exponential memory function to demonstrate their equavalence. The common parameters; $Q$, $U$, $D_L$ ,$\epsilon$, $\alpha$, were set as 3 cms, 0.5 m/s, 0.1 $m^2/s$, 0.1, and $10^{-3}$ $s^{-1}$. Grid size was set as 10 m and the concenrtration was computed every 10 sec for 20,000 sec. The simulation results were compared at 1, 2, 3, 5 km dowmstream from the upstream boundary (see Figure 18). The simulation results showed nearly identical breakthrough curves. As Figure 19 shows, te minor differences is attributed to the grid depencency of the numerical model of the TSM in that the CDE does not discretize the spatial distance.

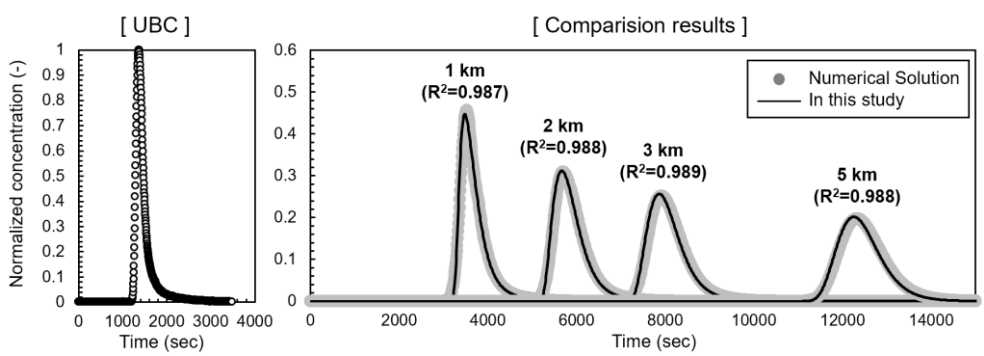


Figure 18. Comparison results of simulations from TSM and CDE.

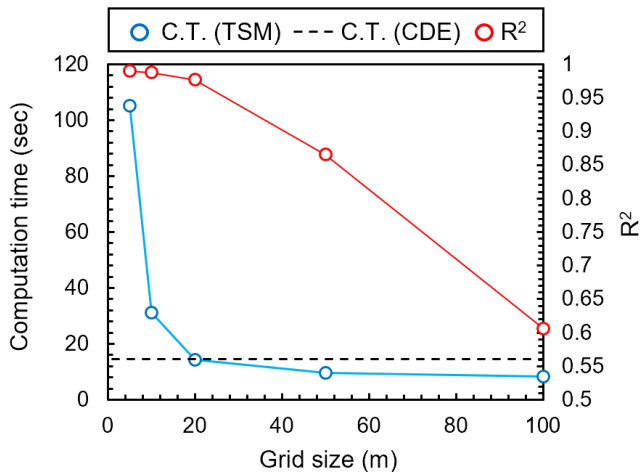


Figure 19. Grid dependency test

3.4 Biodegradation of chemicals in streams

Even though many solute transport analyses have been conducted in recent decades, few of these studies attempted to analyze reactive transport of chemicals as it is difficult to use toxic chemicals in a field test due to safety concerns. Most chemicals are inherently reactive in water. For example, methyl isocyanate is extremely toxic, but cannot be subjected to study since half of them is consumed in few minutes in excess water (Castro et al., 1985). Some hydrogen compounds dissociate or ionize almost completely in water. Some compounds with high vapor pressure or high Henry's law constant may lose their mass when flowing downstream in a river due to their volatility. Therefore, the models need to consider these reaction characteristics to accurately predict the behavior of chemicals in rivers. In order to meet these needs, the OTIS-P (Runkel and Broshears, 1991; Runkel and Chapra, 1993; Runkel, 1998;

Gooseff et al., 2005) includes a sorption algorithm and first-order decay terms on the governing equation of the Transient Storage Model (TSM). The TSM is the most prominent and popular model because it can accurately simulate the skewness of a breakthrough curve (BTC) (Bencala and Walters, 1983). Afterwards Gooseff et al. (2005) referred to the expanded model of TSM as the Reactive Solute Transport Model (RSTM). In their study, Gooseff et al. (2005) estimated the first-order decay parameters using an optimization method with experimental data on nitrogen dioxide from a tracer test in Green Creek, Antarctica. The sorption parameter was set to an arbitrary value. Likewise, O'Connor et al. (2010) employed the improved inverse model to estimate the decay parameters. Haggerty et al. (2009) used resazurin as a smart tracer to provide additional biochemical information in streams. These efforts to estimate the reaction parameters that yield the best-fitting output have confirmed the validity of the first-order decay terms. However, the methods of parameter estimation have a practical limitation in that the parameters optimized for one chemical cannot be applied to another type of chemical. To address the above limitation, the current study attempts to present practical methods for reaction analysis of chemicals in rivers. The governing equations of the RSTM were manipulated. The numerical model was constructed using the Finite Difference Method (FDM) and Crank-Nicolson method. In addition, an analytical solution of the manipulated governing equations was devised in order to verify the numerical model. To determine the reactivity parameters, the inherent properties of chemicals were conjugated based on the appropriate theoretical and empirical methods. Since an estimation of conservative transport parameters

should precede reactive transport parameter estimation (Wagner and Harvey, 1999), tracer tests using Rhodamin WT were conducted at Gam Creek, South Korea in 2019 and 2020. The test bed was also subjected to the reactive transport simulations. By extension, the simulation results were used for the sensitivity analysis of the model with respect to the decay parameters. A flow chart of model development and validation is shown in Fig. 1.

Organic chemicals in natural rivers commonly lose mass due to biochemical reactions, and the remaining chemical concentration can be plotted logarithmically with respect to time by first-order kinetics. This first-order kinetics is also referred to as a half-life kinetics because the half-life represents the elapsed time for a chemical to halve (Alexander, 1999). The biodegradation half-life has a relation with the first-order biodegradation rate, $\lambda_b$.

The EPI Suite from the US EPA offers several biodegradation models, in which an indication of biodegradation rate is provided in relative terms of time range, such as hours, days, and so on (Boethling et al., 1994). One of the models, BIOHCWIN, can estimate the biodegradation half-life using hydrocarbon content (Howard et al., 2005). The provided half-life value was converted to the biodegradation rate using Eq. (13).

# CHAPTER IV

# RESULTS AND DISCUSSIONS

## 4.1 Tracer behavior in a stream

As seen in Figure 13, the shape of tracer cloud was highly skewed with tails along the banks. Considering the bed materials and channel morphology of the testbed, it is attributed to the storage zones of shallow areas and hyporheic zones. The tailing effects also can be observed in the measured concentration-time curves in Figure 20. To demonstrate the limitation in accuracy of Gaussian approximation, the observed concentration-time curves were compared to ADE and TSM simulations. The model parameters were determined that yield best-fit curves to observations, and summarized in Table 5. It is noticeable that the longitudinal dispersion coefficients of ADE are much larger than those of TSM. It is because the ADE cannot distinguish the dispersion effect from shear flow and storage effect, so that the dispersion coefficients of ADE contains the dispersion effect by storage zones as well. Likewise, the mean velocities of the ADE were slower that those of TSM. In sum, the storage term and parameters of TSM partially play a role of delaying the tracer transport and spreading its cloud.

Table 5. Optimized parameters of ADE and TSM

| | ADE | | TSM | | | |
|---|---|---|---|---|---|---|
| | $D_L$ ($m^2/s$) | $U$ (m/s) | $D_L$ ($m^2/s$) | $U$ (m/s) | $\epsilon$ (-) | $\alpha$ (/sec) |
| Reach 1 | 9.420 | 0.556 | 0.564 | 0.605 | 0.227 | 0.00038 |
| Reach 2 | 4.508 | 0.611 | 0.591 | 0.644 | 0.157 | 0.00029 |
| Reach 3 | 23.41 | 0.293 | 4.885 | 0.355 | 0.337 | 0.00015 |

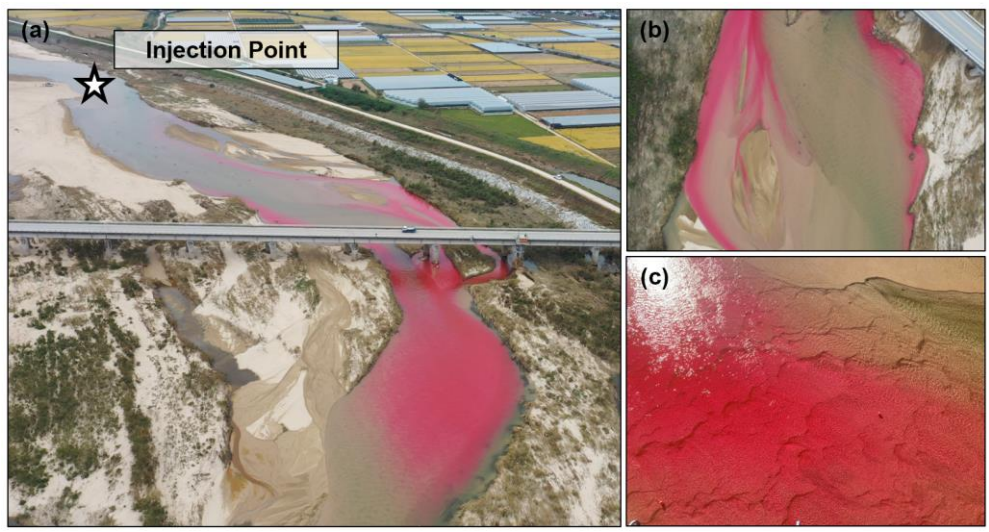


Figure 20. View of tracer behavior propagating upon dune-bedded river morphology (a) Transport of tracer cloud; (b) Tailing due to storage zone (c) Dune-shape streambed composed of sand substrate with little vegetation.

Such limitation of the ADE can be seen in the concentration curve simulation (see Figure 21 & 22). By incorporating the storage effect into the ADE, the simulation accuracy was improved. Quantitative accuracy comparison of simulation of the ADE and TSM were summarized in Table 6.

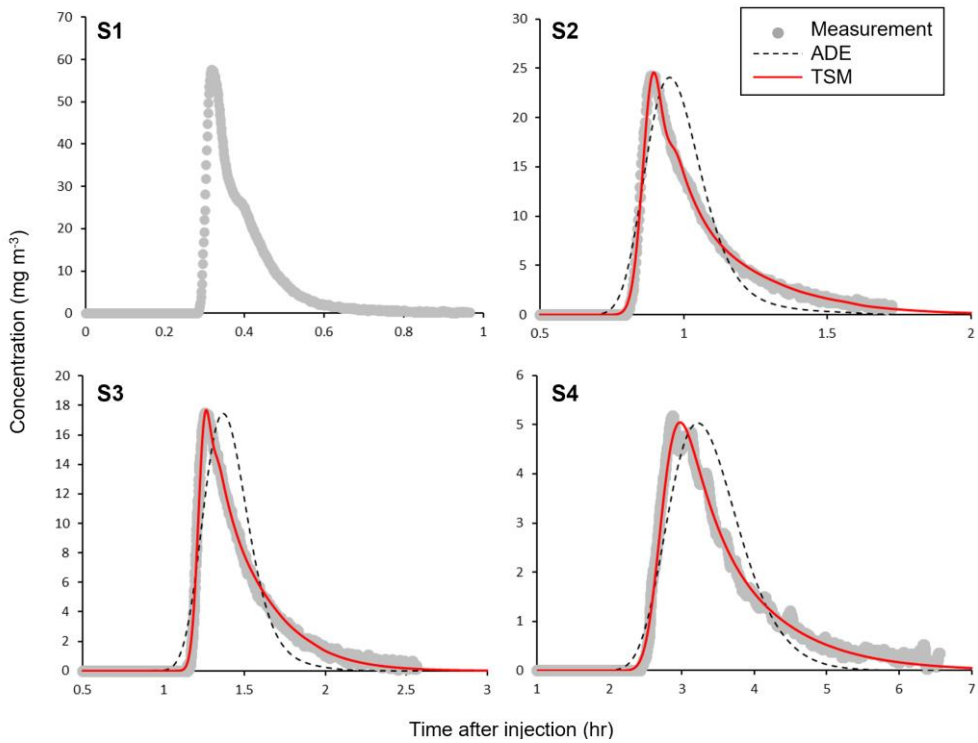


Figure 21. Concentration-time curves observed at tracer test and simulated with ADE and TSM.

Table 6. Accuracy comparison between the simulations of ADE and TSM

| | ADE | | TSM | |
|---|---|---|---|---|
| | $R^2$ | RMSE | $R^2$ | RMSE |
| S2 | 0.893 | 0.893 | 0.959 | 0.209 |
| S3 | 0.860 | 0.860 | 0.967 | 0.177 |
| S4 | 0.888 | 0.888 | 0.963 | 0.145 |

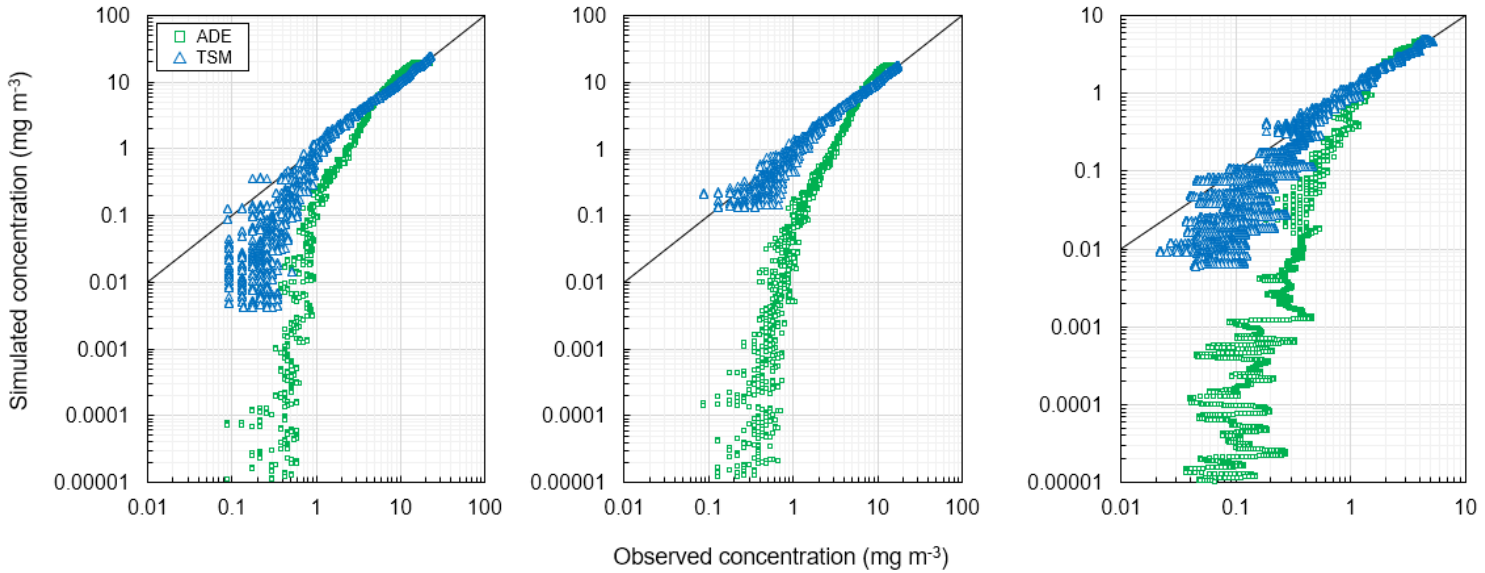


Figure 22. Concentration values along the falling limbs

On this tracer behavior, we applied the Convolutional Decomposition Equation delineated in section 3.2. Figure 23 showed how equation (6) functions combining with equation (13) by applying to the tracer observations. When simulated with the Fickian approximation of $r_f$ delineated in section 2.2, 0.406, 0.954, 0.188 of $R^2$ were estimated at S2, S3, and S4, respectively. This results indicated that the Elder's shear dispersion underestimated the actual tracer cloud separation in the Gam Creek. This study attributed such additional separation to the storage effect. When this results were convolved by $\Phi$ with exponential $\varphi$ ($\alpha$ and $\epsilon$ were optimized), they became closer to the tracer behavior with 0.909, 0.996, 0.959 of $R^2$, respectively, indicating that $\Phi$ can represent the time-dependent storage effect if the storage system is linear.

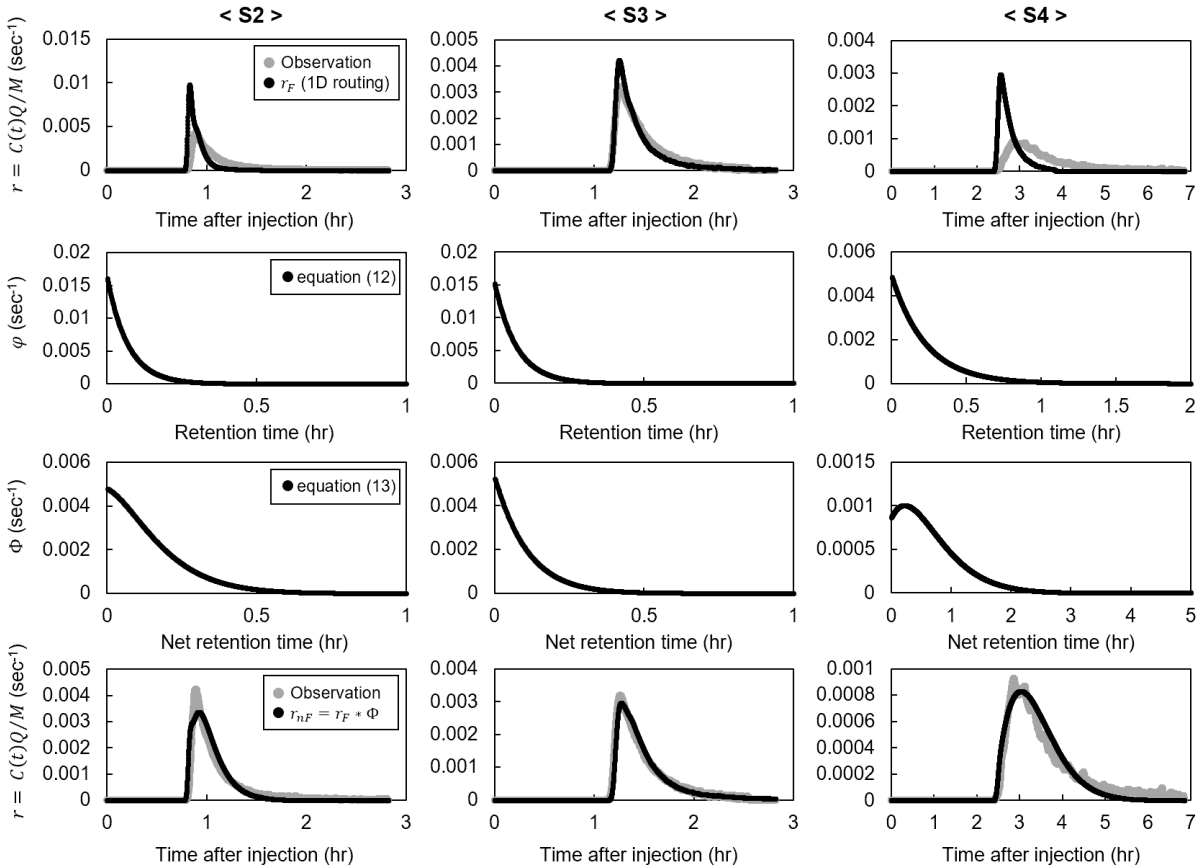


Figure 23. Tracer observations and simulation results of equation (6) at S2, S3, and S4.

Also, we should note that the width of the testbed could be too large to apply the one-dimensional analysis, resulting the breakthrough curve variation in transverse direction (see Figure 24) shows. In this case the cross-sectional averaged concentration cannot represent the concentration of the cross-section. However, since this study is interested in the travel time only, not concentration, the mass or concentration value of the curves were normalized. Therefore, such discrepancy with the conceptual model may not affect the results of this study.

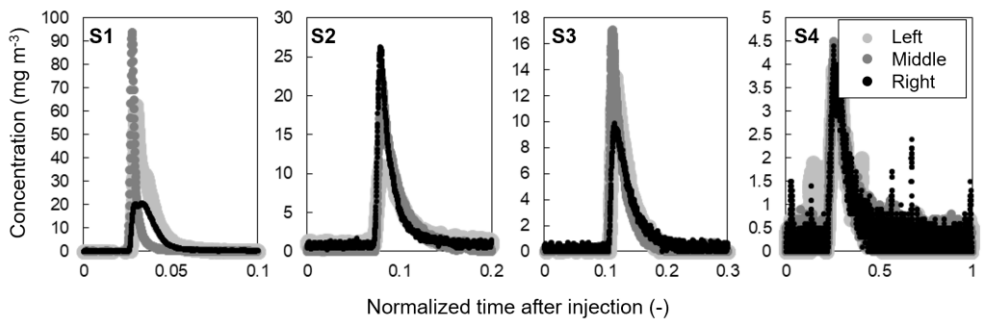


Figure 24. Breakthrough curve variation in transverse direction

## 4.2 Net retention time distribution

Figure 25 shows the deconvolved NRTFs from the tracer test data in varying filtering order. These figures consistently show that the filtering with $N = 1$ was not sufficiently able to block the high-frequency contributions, and thus the resulting NRTFs did not form clear distributions. Meanwhile, the ideal filter, which is the higher order filter, yielded continuously distributed shapes, but they oscillated. As a result, the filtering with $N = 3$ yielded the least distorted and thus most reliable NRTFs. Although the filtered $\Phi$ has negative values, since the NRTF is a probability density function, those negative values do not deeply affect evaluation of the temporal expectation. In comparison of the results, the NRTF of Reach 2 was distributed in a relatively low range of retention time. In particular, it peaked at zero, and as the retention time increased, gradually attenuated. This revealed that Reach 2 had the lowest possibility of trapping tracer particles, which has links to the lowest potential storage effect among the sub-reaches. In contrast, that of Reach 3 was relatively shifted towards large retention time range, and peaked at ~1,000 s, indicating that Reach 3 had more storage effect-inducing environments than the others.

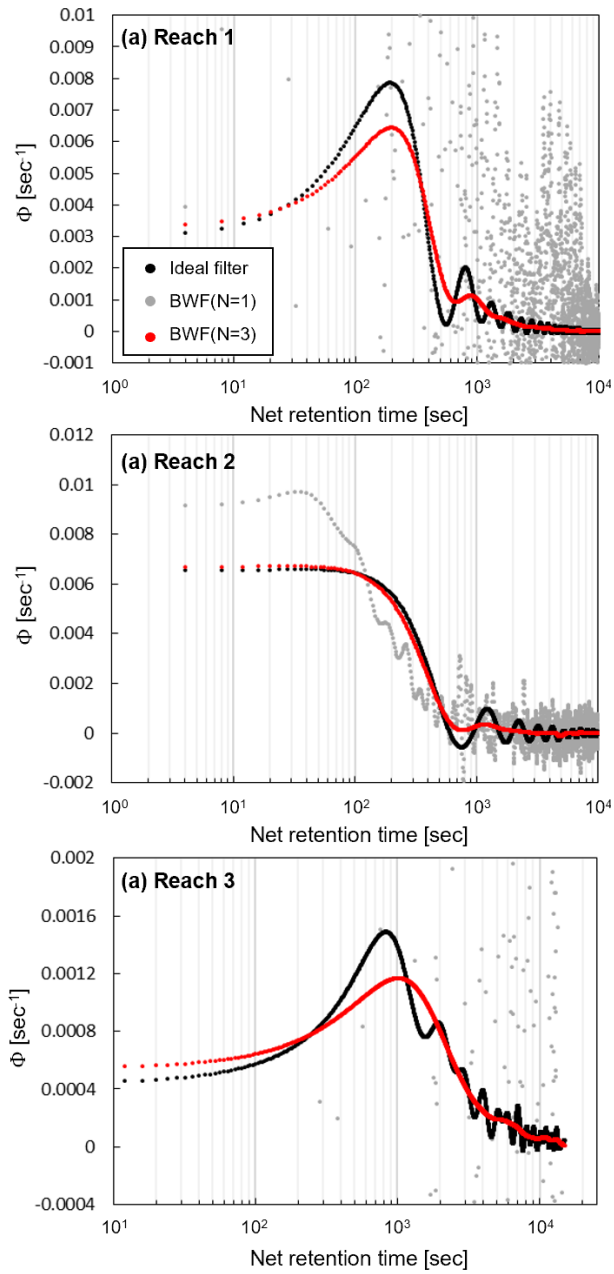


Figure 25. Estimated NRTFs from tracer test data in varying transition smoothness.

The estimated NRTFs were so artificially manipulated that the original distribution of observations could be distorted. To estimate the degree of distortion and demonstrate the validity of the deconvolved NRTFs, the original $\widetilde{r_{nF}}$ values were re-calculated from the filtered NRTFs by equation (2). Figure 10 was plotted in logarithmic scale of y-axis to see the late-time behavior of $\widetilde{r_{nF}}$. The result showed that the filtered data were well-fitted to the original data, except the tail part of S4. At each section, the determination coefficients ($R^2$) were estimated as 0.999, 0.997, and 0.996, respectively, as plotted in Fig. 26. Therefore, the estimated NRTFs preserved the unmarred information of the original observations, and at the same time successively represented the temporal behavior of the tracer within the storage zones.

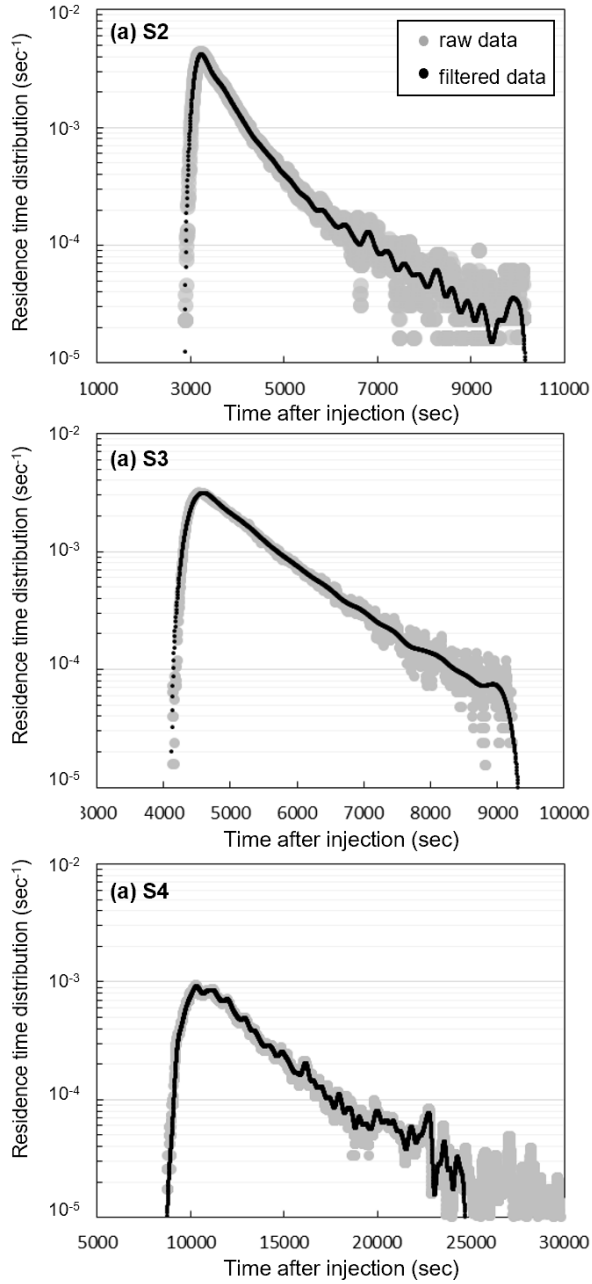


Figure 26. Validation of the deconvolved NRTFs by comparison with the observations.

# CHAPTER V

# APPLICATION

## 5.1 Evaluation of TSM simulation

Based on the underlying reliability of the Fickian transport simulation with the Routing model, the NRTF estimation does not require any premise, such as the uniformity and homogeneity of the storage zones along the stream. In this study, the TSM's conceptualization for the storage system and transient storage parameters were evaluated using the estimated NRTFs. There were two cases of TSM simulations: The first case (Case 1) was that the four parameters; $U$, $D_L$, $\epsilon$, and $\alpha$ defined in section 2.3, were determined that yielded the best-fitted breakthrough curve to observations using the optimization scheme of Noh et al. (2019, 2021), which is the classical technique for transient storage parameter determination (Choi et al., 2020; Femeena et al., 2020; Jackson et al., 2013; Kim et al., 2021a; Kim et al., 2021b; Rana et al., 2017; Rivord et al., 2014; Rowiński & Piotrowski, 2008; Zaramella et al., 2016). Although high simulation accuracy can be expected from the first case, such roughly determined parameters cannot play each primary role that they were defined to represent. In particular, since the dispersion coefficient, $D_L$, and transient storage parameters, $\epsilon$ and $\alpha$, have similar roles in forming breakthrough curves, of lowering the peak value and increasing the temporal variance, they should thus be separately estimated. In this respect, the second case (Case 2) was that the $U$ was estimated from the advection velocity of the tracer

cloud front, the $D_L$ from Elder's velocity profile-based equation. The remaining two transient storage parameters, $\epsilon$ and $\alpha$, were optimized. Table 7 summarizes the results of those two cases. The comparison results between the sub-reaches in section 5.1 were also revealed in the parameters: In both cases, the largest retention time in Reach 3 and the shortest retention time in Reach 2 were also reflected in their $\epsilon$. In contrast to the similar $U$ of two cases at each sub-reach, noticeable differences in $D_L$ were found. We attributed the larger $D_L$ to the lumped parameter estimation of Case 1, resulting in the storage effect-included $D_L$. In particular, the largest $D_L$ of Reach 3, Case 1, could be attributed to the largest storage effect, as seen in Figure 25c. On the other hand, due to the uniform channel dimensions, Case 2 showed relatively uniform $D_L$ values of the sub-reaches. Instead, larger $\epsilon$ values were estimated than those of Case 1, especially that of Reach 3, representing that spreading of the tracer cloud beyond the Elder's shear dispersion was characterized as storage effect.

Table 7. Estimated transient storage parameters and corresponding $R^2$.

| Case | Sub-reach | $U$ ($m\ s^{-1}$) | $D_L$ ($m^2\ s^{-1}$) | $\epsilon$ (-) | $\alpha$ ($10^{-3}s^{-1}$) | $R^2$ (-) |
|---|---|---|---|---|---|---|
| Case 1 | Reach 1 | 0.605 | 0.568 | 0.227 | 0.376 | 0.996 |
| | Reach 2 | 0.644 | 0.591 | 0.157 | 0.292 | 0.996 |
| | Reach 3 | 0.355 | 4.889 | 0.337 | 0.154 | 0.988 |
| Case 2 | Reach 1 | 0.659 | 0.105 | 0.250 | 1.398 | 0.909 |
| | Reach 2 | 0.642 | 0.107 | 0.142 | 0.541 | 0.996 |
| | Reach 3 | 0.436 | 0.125 | 0.491 | 0.598 | 0.959 |

Figure 27 & 28 plot the simulation results of the two cases. For quantitative comparison of the deconvolved and simulated NRTFs, the expectation of net retention time $\langle \Phi \rangle$ values were computed as 808, 430, and 3,135 s, respectively, as listed in Table 8. From these results, we provided several discussions. As expected, the first case simulations revealed more accurate results in the breakthrough curves. However, their expectation values of the net retention times were underestimated by as much as an average 44.3 %. This was because for Case 1, the longitudinal dispersion coefficients were overestimated much larger than the expected values induced by shear dispersion of Case 2. Therefore, the estimated $\epsilon$ and $\alpha$ were not likely to accurately represent the inherent storage characteristics of the corresponding sub-reach.

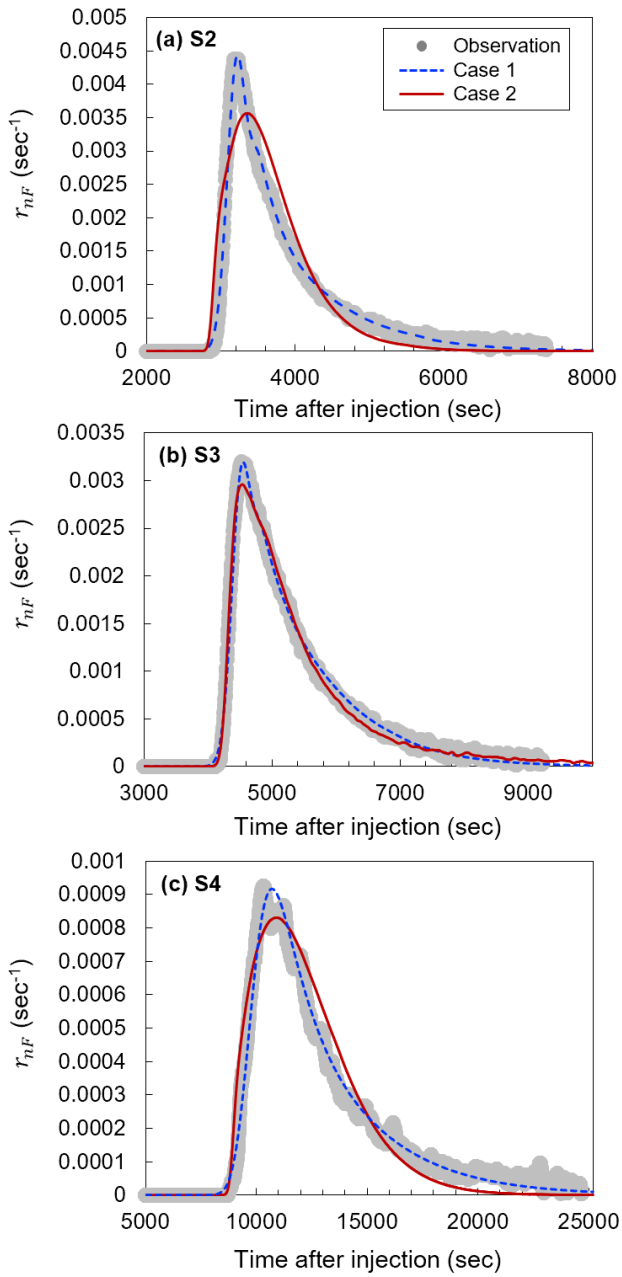


Figure 27. Comparison of residence time distributions of the observations and TSM simulation

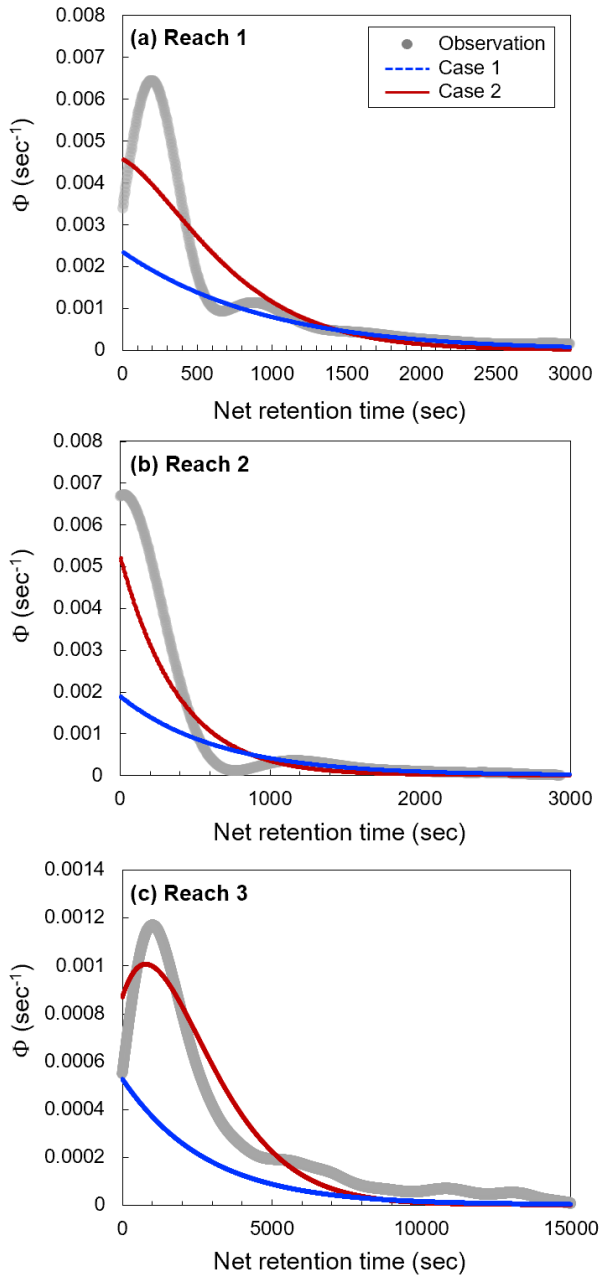


Figure 28. Comparison of the NRTFs of deconvolved observations and TSM simulations.

Table 8. Estimated net retention time expectations at each reach for the three cases.

| | Expectation ($\langle\Phi\rangle$, sec) | | |
|---|---|---|---|
| | Observation | Case 1 (Accuracy[1]) | Case 2 (Accuracy[1]) |
| Reach 1 | 808 | 451 (0.558) | 487 (0.603) |
| Reach 2 | 430 | 198 (0.460) | 361 (0.840) |
| Reach 3 | 3,135 | 971 (0.310) | 2,243 (0.715) |

[1]Accuracy was calculated by $\langle\Phi\rangle_{sim.}/\langle\Phi\rangle_{Obs.}$

From the NRTF simulation results for Case 2 (Figure 15), it is clearly seen that the TSM still cannot accurately reproduce the natural storage effect. Although the transient storage parameters were optimized to the deconvolved NRTFs, poorer accuracies than Case 1 were obtained with an average 0.95 of $R^2$ in the breakthrough curves. As with Case 1, the net retention time expectations were still underestimated by as much as an average 71.9 %. Since we have already demonstrated that the deconvoluted NRTF can produce the reliable $r_{nF}$ without significant distortion, such NRTF discrepancy in Figure 15 was directly related to the $r_{nF}$ discrepancy. Even so, since the estimated $\epsilon$ and $\alpha$ were determined with the best-fitted NRTFs, it can be said that such discrepancy is not from the parameters, but from the structural defect of the TSM. In other words, the exponential $\varphi$ that the TSM has could be a source of the errors, and thus it can be expected that such structural error can be reduced by defining appropriate function of $\varphi$ in equation (13). Specifically, the NRTF of the equation (13) is a weighted superposition of the multi-convolution of negative exponential function $\varphi$ that the TSM has. Hence the resulting NRTF would

similarily distributes, attenuating from $t$ = 0 which is hard to approximate the NRTF with large retention time scale. It was validated in range of $\epsilon$ from $10^{-3}$ to $10^{0}$ and $\alpha$ from $10^{-5}$ to $10^{-3}$ when $T_c$ <1,000 sec (see Figure 29). This result supports the existing argument of the appropriateness of TSM for the fast exchange storage zones.

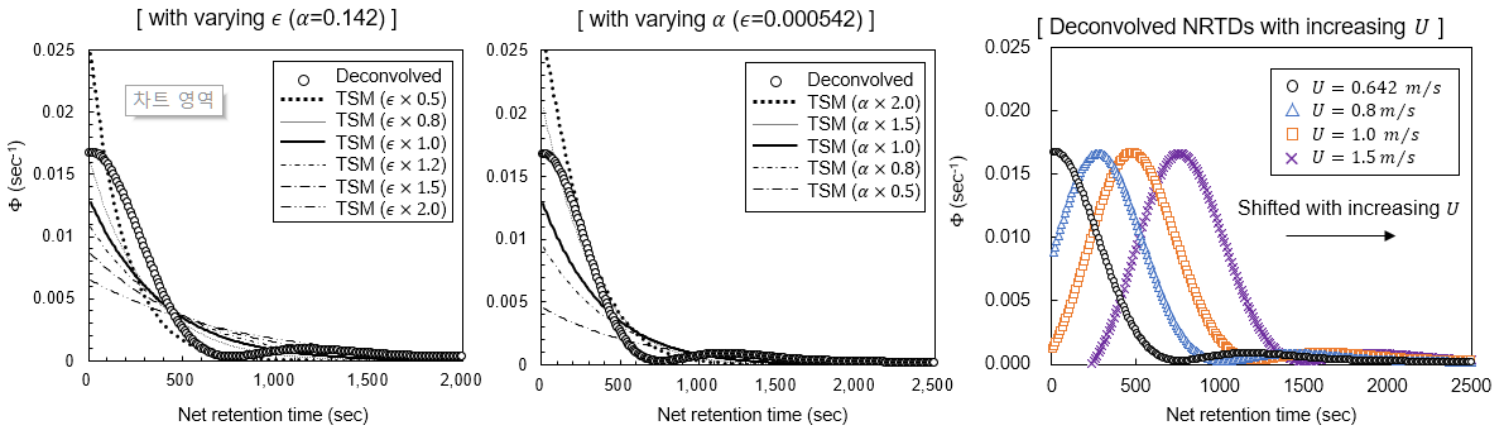


Figure 29. NRTD behavior in varying TSM parameters and increasing retention scale.

5.2 Prediction of biodegradation of chemicals

Based on the deconvolved NRTFs of the tracer, the biodegradation process inside the storage zone was investigated, as recent studies including Gooseff et al. (2011) maintain that the storage zones in streams are potential "hot spots" for biogeochemical activity. The general and acceptable assumption is that the degree of biochemical reaction of organic chemicals in an microbial environment is proportional to its concentration and elapsed time (Aubeneau et al., 2015). In this study, following the work of Kim et al. (2021), the loss rate by biochemical reaction, henceforth termed biodegradation, was inferred from the half-life kinetics that represents the ratio of elapsed time for a chemical staying in a microbial system to its concentration loss (see Figure 30).

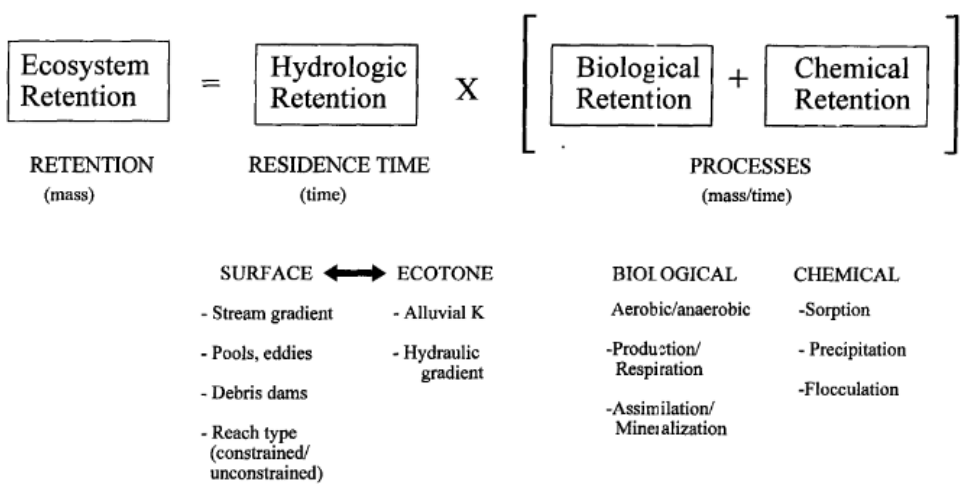


Figure 30. A conceptual model for nutrient retention in stream ecosystems (Valett et al., 1996)

To acquire the biodegradation half-lives of various compounds, Howard et al. (2005) developed the BIOHCWIN model, which is currently employed by the U.S. Environmental Protection Agency (US EPA). This is an estimator of the biodegradation half-lives for chemical compounds using their hydrocarbon structure when no reliable experimental data in environmental media are available. Using the biochemical half-lives of chemicals and the estimated NRTSs, we stochastically predicted how much biodegradation will be incurred within a given fluvial system at varying confidence intervals. Four chemical compounds: toluene, benzene, biphenyl, and naphthalene, were subject to the application. We assumed them to be neutrally buoyant, though such lower-molecular-weight petroleum (aromatic) hydrocarbons generally have lower density than water. Table 9 summarizes their biochemical half-lives and corresponding loss rates, and Figure 31 illustrates them. As a result, it was predicted that the biphenyl of Reach 3 lost its mass more than the subject chemicals of the other reaches, despite its longest half-life. This is because Reach 3 has the longest retention time. Likewise, toluene, which has the fastest reactivity among the chemicals, could be less degraded in Reach 2 than benzene or naphthalene in the other reaches, because it would stay in the storage zones of Reach 2 for a shorter time than the others.

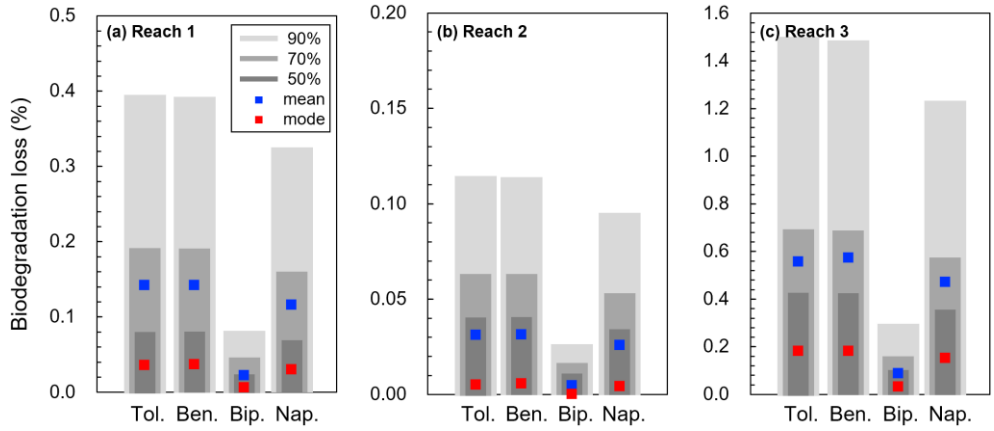


Figure 31. Stochastic estimations of biodegradation loss for toluene, benzene, biphenyl, and naphthalene.

Table 9. Estimations of biodegradation loss for toluene, benzene, biphenyl, and naphthalene in each reach.

| Compounds | Biochemical half-life (days) | Confidence interval | Biodegradation (%) | | |
|---|---|---|---|---|---|
| | | | RC1 | RC2 | RC3 |
| Toluene | 4.4937 | Maximum | 0.035 | 0.005 | 0.1807 |
| | | Expectation | 0.1419 | 0.0312 | 0.5576 |
| | | 50% | 0.006 to 0.066 | 0 to 0.035 | 0.034 to 0.383 |
| | | 70% | 0 to 0.171 | 0 to 0.055 | 0 to 0.627 |
| | | 90% | 0 to 0.367 | 0 to 0.104 | 0 to 1.413 |
| Benzene | 4.5467 | Maximum | 0.0346 | 0.0049 | 0.178 |
| | | Expectation | 0.1402 | 0.0309 | 0.5708 |
| | | 50% | 0.006 to 0.066 | 0 to 0.035 | 0.034 to 0.378 |
| | | 70% | 0 to 0.169 | 0 to 0.054 | 0 to 0.620 |
| | | 90% | 0 to 0.363 | 0 to 0.102 | 0 to 1.397 |
| Biphenyl | 31.0027 | Maximum | 0.0051 | 0 | 0.0262 |
| | | Expectation | 0.0206 | 0.0045 | 0.0837 |
| | | 50% | 0.001 to 0.010 | 0 to 0.005 | 0.005 to 0.056 |
| | | 70% | 0 to 0.025 | 0 to 0.008 | 0 to 0.091 |
| | | 90% | 0 to 0.053 | 0 to 0.015 | 0 to 0.205 |
| Naphthalene | 5.5603 | Maximum | 0.0283 | 0.004 | 0.146 |
| | | Expectation | 0.1146 | 0.0253 | 0.4668 |
| | | 50% | 0.005 to 0.054 | 0 to 0.028 | 0.028 to 0.309 |
| | | 70% | 0 to 0.138 | 0 to 0.044 | 0 to 0.507 |
| | | 90% | 0 to 0.297 | 0 to 0.084 | 0 to 1.142 |

# CHAPTER IV

# CONCLUSIONS

Since the NRTF defined in this study represents the inherent storage characteristics of natural streams without assumptions in the form of storage zones, it is valuable for understanding and quantifying the time-dependent storage effect. The present study aimed at estimating the least-distorted NRTF from tracer test data. As a result, the NRTFs were successfully estimated using the signal deconvolution technique with the Butterworth filter. In addition, in-depth analyses were conducted on the (1) evaluation of storage mechanism modeling of TSM, and (2) stochastic prediction of biodegradation in a stream for various organic chemicals.

From the current study, four key conclusions were derived. First, the NRTF of the stream was successfully estimated from tracer test data. The problematic high-frequency variability of the observed data was controlled using low-pass filter, and the undesired Gibbs phenomenon was restrained by smoothing the response of the filter transition. The key to deconvolution was the appropriate determination of the filtering order and the cutoff frequency. In this study, the filtering order of 3 yielded the least-distorted NRTFs. However, since the global applicability of the filtering parameters has yet to be proved, rigorous care should be taken in the filter parameter determination, depending on the data.

Second, over the last few decades, many studies have demonstrated the simulation accuracy of the TSM with breakthrough curve optimization techniques

(Gooseff et al., 2005; Rivord et al., 2014; Kim et al., 2021). However, this study quantitatively revealed that such TSM simulation underestimated the inherent storage effect of the reach that was not seen in the breakthrough curves. That is, the accurate breakthrough curve simulation does not directly indicate the TSM's accuracy. In this respect, the NRTFs can be valuable tools for evaluation of the one-dimensional storage system modeling.

Third, as the retention time scale of the channel increases, the distribution of NRTFs will be shifted toward large time scale. Accordingly, due to the exponential function of φ embedded in the TSM, it will become harder to fit the large time scale NRTFs of natural streams with the TSM simulation. In other words, the longer the retention time scale that the channel has, the poorer the simulation results that the TSM is likely to yield. Thus, this result well demonstrated the limitation of the TSM stated by Marion et al. (2008). Such evaluation of storage system modeling using the deconvolved NRTFs can be applied to other existing models.

Fourth, once how much time organic chemicals were trapped in the storage zone is identified, we can quantify the chemicals' activity occurring within the storage zone. In this study, using the chemicals' inherent loss rate by biogeochemical activity, biodegradation was estimated. As expected, if the chemical has a short biochemical half-life, or the retention time of the channel was long, high biodegradation was estimated. In addition, since the NRTF is a pdf with respect to retention time, the biodegradation can also be estimated in the pdf, and thus we can estimate the loss rate

with confidence interval that has less uncertainty. Such application could have errors by variation of temperature, pH, microbial populations, and so forth. Although such chemical uncertainty still remains, the probabilistic estimation of net retention time in this study could reduces the uncertainty in anomalous transport of chemicals in streams.

The reliability of the estimated NRTFs was closely related to the accepted current velocity and dispersion coefficient. Such flow parameters should be representable for what they were physically supposed to be: $U$ is the mean advective velocity by river current, and $D_L$ is the longitudinal dispersion coefficient by shear dispersion. We estimated both parameters in this respect, and thus the effects beyond them (defined as the storage effect) are included in the deconvolved NRTFs and the transient storage parameters. This being so, if the transient storage parameters cannot accurately shape the estimated NRTF, the difference is attributed to structural error of the model. Moreover, the existing mathematical formulae for storage mechanism can be evaluated with the deconvolved NRTFs, as we have done with TSM. This NRTF would better represent the storage system than the breakthrough curve tails due to the successful exclusion of flow dynamics.

# REFERENCES

Aubeneau, A.F., Drummond, J.D., Schumer, R., Bolster, D., Tank, J.L., Packman, A.I., 2015. Effects of benthic and hyporheic reactive transport on breakthrough curves. Freshw. Sci. 34, 301–315. https://doi.org/10.1086/680037

Baek, D., Seo, I.W., Kim, J.S., Nelson, J.M., 2019. UAV-based measurements of spatio-temporal concentration distributions of fluorescent tracers in open channel flows. Adv. Water Resour. 127, 76–88. https://doi.org/10.1016/j.advwatres.2019.03.007

Bendat, J.S., Piersol, A.G., 2000. Random data: analysis and measurement procedures, 3rd editio. ed. Wiley & Sons, Inc., New York.

Boano, F., Harvey, J.W., Marion, A., Packman, A.I., Revelli, R., Ridolfi, L., Wörman, A., 2014. Hyporheic flow and transport processes: Mechanisms, models, and biogeochemical implications. Rev. Geophys. 52, 603–679. https://doi.org/10.1002/2012RG000417

Boano, F., Packman, A.I., Cortis, A., Revelli, R., Ridolfi, L., 2007. A continuous time random walk approach to the stream transport of solutes. Water Resour. Res. 43, 1–12. https://doi.org/10.1029/2007WR006062

Bottacin-Busolin, A., Dallan, E., Marion, A., 2021. STIR-RST: A Software tool for reactive smart tracer studies. Environ. Model. Softw. 135, 104894.

https://doi.org/10.1016/j.envsoft.2020.104894

Bottacin-Busolin, A., Marion, A., Musner, T., Tregnaghi, M., Zaramella, M., 2011. Evidence of distinct contaminant transport patterns in rivers using tracer tests and a multiple domain retention model. Adv. Water Resour. 34, 737–746. https://doi.org/10.1016/j.advwatres.2011.03.005

Cardenas, M.B., 2007. Potential contribution of topography-driven regional groundwater flow to fractal stream chemistry: Residence time distribution analysis of Tóth flow. Geophys. Res. Lett. 34, 1–5. https://doi.org/10.1029/2006GL029126

Chen, P.Y., Sivan, Y., 2021. Resolving the Gibbs phenomenon via a discontinuous basis in a mode solver for open optical systems. J. Comput. Phys. 429, 110004. https://doi.org/10.1016/j.jcp.2020.110004

Cheong, T.S., Seo, I.W., 2003. Parameter estimation of the transient storage model by a routing method for river mixing processes. Water Resour. Res. 39. https://doi.org/10.1029/2001WR000676

Cheong, T.S., Younis, B.A., Seo, I.W., 2007. Estimation of key parameters in model for solute transport in rivers and streams. Water Resour. Manag. 21, 1165–1186. https://doi.org/10.1007/s11269-006-9074-7

Choi, S.Y., Seo, I.W., Kim, Y.O., 2020. Parameter uncertainty estimation of transient storage model using Bayesian inference with formal likelihood

based on breakthrough curve segmentation. Environ. Model. Softw. 123, 104558. https://doi.org/10.1016/j.envsoft.2019.104558

Cox, M.H., Mendez, G.O., Kratzer, C.R., Reichard, E.G., 2003. Evaluation of Tracer Tests Completed in 1999 and 2000 on the Upper Santa Clara river, Los Angeles and Ventura Counties, California 92.

Day, T.J., 1975. Longitudinal dispersion in natural channels. Water Resour. Res. 11, 909–918. https://doi.org/10.1029/WR011i006p00909

De Smedt, F., Brevis, W., Debels, P., 2005. Analytical solution for solute transport resulting from instantaneous injection in streams with transient storage. J. Hydrol. 315, 25–39. https://doi.org/10.1016/j.jhydrol.2005.04.002

Drummond, J.D., Aubeneau, A.F., Packman, A.I., 2014. Stochastic modeling of fine particulate organic carbon dynamics in rivers. Water Resour. Resear50 50, 4341–4356. https://doi.org/10.1002/2013WR014665.

Drummond, J.D., Covino, T.P., Aubeneau, A.F., Leong, D., Patil, S., Schumer, R., Packman, A.I., 2012. Effects of solute breakthrough curve tail truncation on residence time estimates: A synthesis of solute tracer injection studies. J. Geophys. Res. Biogeosciences 117, 1–11. https://doi.org/10.1029/2012JG002019

Drummond, J.D., Larsen, L.G., Gonzalez-Pinzon, R., Packman, A.I., Harvey, J.W., 2017. Fine particle retention within stream storage areas at base flow and in

response to a storm event. Water Resour. Res. 53, 5690–5705. https://doi.org/10.1111/j.1752-1688.1969.tb04897.x

Duchon, C.E., 1979. Lanczos filtering in one and two dimensions. J. Appl. Meteorol. Climatol. 18, 1016–1022.

Elliott, A.H., Brooks, N.H., 1997. Transfer of nonsorbing solutes to a streambed with bed forms: Theory. Water Resour. Res. 33, 123–136. https://doi.org/10.1029/96WR02784

Elliott, A.H., Brooks, N.H., Keck, W.M., 1997. Transfer of nonsorbing solutes to a streambed with bed forms: Laboratory experiment. Water Resour. Res. 33, 137–151.

Femeena, P. V., Chaubey, I., Aubeneau, A., McMillan, S., Wagner, P.D., Fohrer, N., 2019. Simple regression models can act as calibration-substitute to approximate transient storage parameters in streams. Adv. Water Resour. 123, 201–209. https://doi.org/10.1016/j.advwatres.2018.11.010

Femeena, P. V., Chaubey, I., Aubeneau, A., McMillan, S.K., Wagner, P.D., Fohrer, N., 2020. Developing an improved user interface for a physically-based stream solute transport model. Environ. Model. Softw. 129, 104715. https://doi.org/10.1016/j.envsoft.2020.104715

Fischer, H.B., List, E.J., Koh, R.C.Y., Imberger, J., Brooks, N.H., 1979. Mixing in inland and coastal waters.

Gibbs, J.W., 1898. Fourier's series. Nature 59, 200–200.

Gooseff, M.N., Benson, D.A., Briggs, M.A., Weaver, M., Wollheim, W., Peterson, B., Hopkinson, C.S., 2011. Residence time distributions in surface transient storage zones in streams: Estimation via signal deconvolution. Water Resour. Res. 47, 1–7. https://doi.org/10.1029/2010WR009959

Gooseff, M.N., Briggs, M.A., Bencala, K.E., McGlynn, B.L., Scott, D.T., 2013. Do transient storage parameters directly scale in longer, combined stream reaches? Reach length dependence of transient storage interpretations. J. Hydrol. 483, 16–25. https://doi.org/10.1016/j.jhydrol.2012.12.046

Gooseff, M.N., LaNier, J., Haggerty, R., Kokkeler, K., 2005. Determining in-channel (dead zone) transient storage by comparing solute transport in a bedrock channel-alluvial channel sequence, Oregon. Water Resour. Res. 41, 1–7. https://doi.org/10.1029/2004WR003513

Gooseff, M.N., Wondzell, S.M., Haggerty, R., Anderson, J., 2003. Comparing transient storage modeling and residence time distribution (RTD) analysis in geomorphically varied reaches in the Lookout Creek basin, Oregon, USA. Adv. Water Resour. 26, 925–937. https://doi.org/10.1016/S0309-1708(03)00105-2

Guymer, I., Stovin, V.R., 2011. One-Dimensional Mixing Model for Surcharged Manholes. J. Hydraul. Eng. 137, 1160–1172.

https://doi.org/10.1061/(asce)hy.1943-7900.0000422

Haggerty, R., McKenna, S.A., Meigs, L.C., 2000. On the late-time behavior of tracer test breakthrough curves. Water Resour. Res. 36, 3467–3479. https://doi.org/10.1029/2000WR900214

Haggerty, R., Wondzell, S.M., Johnson, M.A., 2002. Power-law residence time distribution in the hyporheic zone of a 2nd-order mountain stream. Geophys. Res. Lett. 29, 18-1-18–4. https://doi.org/10.1029/2002GL014743

Hart, D.R., 1995. Parameter Estimation and Stochastic Interpretation of the Transient Storage Model For Solute Transport in Streams. Water Resour. Res. 31, 323–328. https://doi.org/10.1029/94WR02739

Hart, J.R., Guymer, I., Sonnenwald, F., Stovin, V.R., 2016. Residence Time Distributions for Turbulent, Critical, and Laminar Pipe Flow. J. Hydraul. Eng. 142, 04016024. https://doi.org/10.1061/(asce)hy.1943-7900.0001146

Howard, P., Meylan, W., Aronson, D., Stiteler, W., Tunkel, J., Comber, M., Parkerton, T.F., 2005. A new biodegradation prediction model specific to petroleum hydrocarbons. Environ. Toxicol. Chem. 24, 1847–1860. https://doi.org/10.1897/04-453R.1

Jackson, T.R., Haggerty, R., Apte, S. V., 2013. A fluid-mechanics based classification scheme for surface transient storage in riverine environments: Quantitatively separating surface from hyporheic transient storage. Hydrol.

Earth Syst. Sci. 17, 2747–2779. https://doi.org/10.5194/hess-17-2747-2013

Jackson, T.R., Haggerty, R., Apte, S. V., Coleman, A., Drost, K.J., 2012. Defining and measuring the mean residence time of lateral surface transient storage zones in small streams. Water Resour. Res. 48, 1–20. https://doi.org/10.1029/2012WR012096

Kim, B., Seo, I.W., Kwon, S., Jung, S.H., Choi, Y., 2021a. Modelling one-dimensional reactive transport of toxic contaminants in natural rivers. Environ. Model. Softw. 137, 104971. https://doi.org/10.1016/j.envsoft.2021.104971

Kim, B., Seo, I.W., Kwon, S., Jung, S.H., Yun, S.H., 2021b. Analysis of solute transport in rivers using a stochastic storage model. J. Korea Water Resour. Assoc. 54, 335–345. https://doi.org/10.3741/JKWRA.2021.54.5.335

Knapp, J.L.A., Kelleher, C., 2020. A Perspective on the Future of Transient Storage Modeling: Let's Stop Chasing Our Tails. Water Resour. Res. 56, 1–7. https://doi.org/10.1029/2019WR026257

Krishnan, D., Fergus, R., 2009. Fast image deconvolution using hyper-laplacian priors. Adv. Neural Inf. Process. Syst. 22, 1033–1041.

Kundur, D., Hatzinakos, D., 1996. Blind image deconvolution. IEEE Signal Process. Mag. 13, 43–61.

Marion, A., Bellinello, M., Guymer, I., Packman, A., 2002. Effect of bed form

geometry on the penetration of nonreactive solutes into a streambed. Water Resour. Res. 38, 27-1-27–12. https://doi.org/10.1029/2001wr000264

Marion, A., Zaramella, M., 2005. A residence time model for stream-subsurface exchange of contaminants. Acta Geophys. Pol. 53, 527–538.

Marion, A., Zaramella, M., Bottacin-Busolin, A., 2008. Solute transport in rivers with multiple storage zones: The STIR model. Water Resour. Res. 44, 1–10. https://doi.org/10.1029/2008WR007037

Meerschaert, M.M., Zhang, Y., Baeumer, B., 2008. Tempered anomalous diffusion in heterogeneous systems. Geophys. Res. Lett. 35, 1–5. https://doi.org/10.1029/2008GL034899

Mignot, E., Cai, W., Polanco, J.I., Escauriaza, C., Riviere, N., 2017. Measurement of mass exchange processes and coefficients in a simplified open-channel lateral cavity connected to a main stream. Environ. Fluid Mech. 17, 429–448. https://doi.org/10.1007/s10652-016-9495-7

Noh, H., Baek, D., Seo, I.W., 2019. Analysis of the applicability of parameter estimation methods for a transient storage model. J. Korea Water Resour. Assoc. 52, 681–695. https://doi.org/10.3741/JKWRA.2019.52.10.681

Noh, H., Kwon, S., Seo, I.W., Baek, D., Jung, S.H., 2021. Multi-gene genetic programming regression model for prediction of transient storage model parameters in natural rivers. Water 13, 76.

https://doi.org/10.3390/w13010076

Payn, R.A., Gooseff, M.N., Benson, D.A., Cirpka, O.A., Zarnetske, J.P., Bowden, W.B., McNamara, J.P., Bradford, J.H., 2008. Comparison of instantaneous and constant-rate stream tracer experiments through non-parametric analysis of residence time distributions. Water Resour. Res. 44, 1–10. https://doi.org/10.1029/2007WR006274

Pederson, F.B., 1977. Prediction of longitudinal dispersion in natural streams. Ser. Pap. 14.

Piotrowski, A., Wallis, S.G., Napiórkowski, J.J., Rowiński, P.M., 2007. Evaluation of 1-D tracer concentration profile in a small river by means of Multi-Layer Perceptron Neural Networks. Hydrol. Earth Syst. Sci. 11, 1883–1896. https://doi.org/10.5194/hess-11-1883-2007

Rana, S.M.M., Scott, D.T., Hester, E.T., 2017. Effects of in-stream structures and channel flow rate variation on transient storage. J. Hydrol. 548, 157–169. https://doi.org/10.1016/j.jhydrol.2017.02.049

Rivord, J., Laurel Saito, P.E., Miller, G., Stoddard, S.S., 2014. Modeling contaminant spills in the truckee river in the western United States. J. Water Resour. Plan. Manag. 140, 343–354. https://doi.org/10.1061/(ASCE)WR.1943-5452.0000338

Rowiński, P.M., Piotrowski, A., 2008. Estimation of parameters of the transient

storage model by means of multi-layer perceptron neural networks. Hydrol. Sci. J. 53, 165–178. https://doi.org/10.1623/hysj.53.1.165

Rowiński, P.M., Piotrowski, A., Napiórkowski, J.J., 2005. Are artificial neural network techniques relevant for the estimation of longitudinal dispersion coefficient in rivers? Hydrol. Sci. J. 50, 175–187. https://doi.org/10.1623/hysj.50.1.175.56339

Runkel, R.L., 2015. On the use of rhodamine WT for the characterization of stream hydrodynamics and transient storage. Water Resour. Res. 51, 6125–6142. https://doi.org/10.1002/2015WR017201

Runkel, R.L., 1998. One-dimensional transport with inflow and storage (otis): a solute transport model for streams and rivers. Water-Resources Investig. Rep. 98-4018 0–80. https://doi.org/Cited By (since 1996) 47\nExport Date 4 April 2012

Sahay, R.R., 2012. Predicting Transient Storage Model Parameters of Rivers by Genetic Algorithm. Water Resour. Manag. 26, 3667–3685. https://doi.org/10.1007/s11269-012-0092-3

Sandoval, J., Mignot, E., Mao, L., Pastén, P., Bolster, D., Escauriaza, C., 2019. Field and Numerical Investigation of Transport Mechanisms in a Surface Storage Zone. J. Geophys. Res. Earth Surf. 124, 938–959. https://doi.org/10.1029/2018JF004716

Schumer, R., Benson, D.A., Meerschaert, M.M., Baeumer, B., 2003. Fractal mobile/immobile solute transport. Water Resour. Res. 39, 1–12. https://doi.org/10.1029/2003WR002141

Shin, J., Seo, I.W., Baek, D., 2020. Longitudinal and transverse dispersion coefficients of 2D contaminant transport model for mixing analysis in open channels. J. Hydrol. 583, 124302. https://doi.org/10.1016/j.jhydrol.2019.124302

Sonnenwald, F., Stovin, V., Guymer, I., 2015. Deconvolving Smooth Residence Time Distributions from Raw Solute Transport Data. J. Hydrol. Eng. 20, 04015022. https://doi.org/10.1061/(asce)he.1943-5584.0001190

Sonnenwald, F., Stovin, V., Guymer, I., 2014. Configuring Maximum Entropy Deconvolution for the Identification of Residence Time Distributions in Solute Transport Applications. J. Hydrol. Eng. 19, 1413–1421. https://doi.org/10.1061/(asce)he.1943-5584.0000929

Sonnenwald, F., Stovin, V., Guymer, I., 2011. The influence of outlet angle on solute transport in surcharged manholes. … 12th Int. Conf. … 11–16.

Stonedahl, S.H., Harvey, J.W., Detty, J., Aubeneau, A., Packman, A.I., 2012. Physical controls and predictability of stream hyporheic flow evaluated with a multiscale model. Water Resour. Res. 48, 1–15. https://doi.org/10.1029/2011WR011582

Taylor, G.I., 1954. The dispersion of matter in turbulent flow through a pipe. Proc. R. Soc. London. Ser. A. Math. Phys. Sci. 223, 446–468. https://doi.org/10.1098/rspa.1954.0130

Thackston, E.L., Schnelle, K.B.J., 1970. Predicting effects of dead zones on stream mixing. J. Sanit. Eng. Div. 96, 319–331.

Valett, H.M., Morrice, J.A., Dahm, C.N., Campana, M.E., 1996. Parent lithology, surface-groundwater exchange, and nitrate retention in headwater streams. Limnol. Oceanogr. 41, 333–345. https://doi.org/10.4319/lo.1996.41.2.0333

Wallis, S., Manson, R., 2019. Sensitivity of optimized transient storage model parameters to spatial and temporal resolution. Acta Geophys. 67, 951–960. https://doi.org/10.1007/s11600-019-00253-x

Ward, A.S., Payn, R.A., Gooseff, M.N., McGlynn, B.L., Bencala, K.E., Kelleher, C.A., Wondzell, S.M., Wagener, T., 2013. Variations in surface water-ground water interactions along a headwater mountain stream: Comparisons between transient storage and water balance analyses. Water Resour. Res. 49, 3359–3374. https://doi.org/10.1002/wrcr.20148

Weitbrecht, V., Socolofsky, S.A., Jirka, G.H., 2008. Experiments on Mass Exchange between Groin Fields and Main Stream in Rivers. J. Hydraul. Eng. 134, 173–183.

Wörman, A., Packman, A.I., Johansson, H., Jonsson, K., 2002. Effect of flow-

induced exchange in hyporheic zones on longitudinal transport of solutes in streams and rivers. Water Resour. Res. 38, 2-1-2–15. https://doi.org/10.1029/2001wr000769

Wörman, A., Wachniew, P., 2007. Reach scale and evaluation methods as limitations for transient storage properties in streams and rivers. Water Resour. Res. 43, 1–13. https://doi.org/10.1029/2006WR005808

Zaramella, M., Marion, A., Lewandowski, J., Nützmann, G., 2016. Assessment of transient storage exchange and advection-dispersion mechanisms from concentration signatures along breakthrough curves. J. Hydrol. 538, 794–801. https://doi.org/10.1016/j.jhydrol.2016.05.004

Zarnetske, J.P., Gooseff, M.N., Brosten, T.R., Bradford, J.H., McNamara, J.P., Bowden, W.B., 2007. Transient storage as a function of geomorphology, discharge, and permafrost active layer conditions in Arctic tundra streams. Water Resour. Res. 43, 1–13. https://doi.org/10.1029/2005WR004816

# 국문초록

## 자연하천에서 물질 혼합해석을 위한 저장대에서의 정체시간분포 산정

**서울대학교 대학원**
**건설환경공학부**
**김병욱**

자연하천에서 용존물질의 거동은 하천의 지형학적인 요인으로 형성된 저장대의 영향에 의해 흐름 영역의 특성만으로 해석될 수 없다. 이러한 저장대 효과를 분석하기 위해 지난 수십년동안 다양한 구조의 저장대 모형이 제시되어 왔다. 용존물질의 하류이송을 지체시키는 이러한 저장대의 영향을 고려하기 위해, 기존의 1 차원 이송-분산 방정식을 바탕으로 다양한 형태의 저장대 모형이 개념적으로 제시되어 왔다. 이러한 모형의 타당성은 대부분 흐름영역에서 측정한 추적자의 농도-시간 곡선의 실측값으로부터 증명되어 왔다. 하지만, 흐름영역에서의 추적자 거동은 저장대의 영향보다 이송과 분산의 영향에 더욱 민감하기 때문에, 이는 저장대의 영향을 대표하기 어려우며, 저장대 모델링은 저장대의 영향의 실측값으로부터 검증되어야 한다. 하지만, 자연하천의 저장대는 그 형태가 다양하며 경계가 모호하기 때문에 실측값을 얻기 힘든 한계가 있다.

따라서, 본 연구에서는 이송, 분산의 영향과 저장대의 영향을 명시적으로 구분할 수 있는 모형을 제시하고, 역합성곱 기법을 적용하여 흐름영역에서 측정한 추적자의 거동으로부터 이송과 분산의 영향을 제외하여 저장대의 영향만을 측정할 수 있는 방법을 제시하였다. 측정한 저장대의 영향은 가장 대표적인 1 차원 저장대 모형인 Transient Storage Model (TSM)의 모의 결과와 결정된 매개변수의 타당성을 검증하는데 활용되었다. 그 결과 TSM 의 모의는 실제 하천의 저장대의 영향을 44%까지 과소평가하는 결과를 보였다. 또한, 자연하천에서 저장대가 수계 생물화학적 반응의 주요 영역이라는 점을 고려하여, 평가된 정체시간분포를 이용하여 여러 유기화학물질별 생화학적 반응에 의한 감쇠정도를 평가하는데 활용되었다.

주요어: 하천혼합, 저장대모형, 정체시간분포, 추적자 실험, 생화학적반응
학번: 2020-22143